On the stability of strain-rate dependent solids. I-Structural examples

Patrick Massin, Nicolas Triantafyllidis, Yves Leroy

On the stability of strain-rate dependent solids I — Structural examples

P. Massin[a], N. Triantafyllidis[b], Y.M. Leroy[c]

[a]Electricite de France, DEM-MMN, Clamart, France
[b]Department of Aerospace Engineering, The University of Michigan, Ann Arbor, USA
[c]Laboratoire de Mécanique des Solides, Ecole polytechnoque, URM CNRS 7649, Palaiseau, France

Abstract

A linear stability criterion for strain-rate sensitive solids and structures is proposed and validated with the help of two versions of Shanley's column, the first with two discrete supports and the second with a continuous distribution of supports. Linear stability transition is defined by the change in sign of the second derivative with respect to time of the column's angular position evaluated at the onset of perturbation. This criterion pertains to the initiation of instabilities but is not expected to provide information on their long term development. Two parameters influence linear stability: the dimensionless number T, defined as the ratio of the relaxation time of the viscous support to the characteristic loading time, and the perturbation size. It is found that the critical load of principal equilibria, defined for a straight column and a zero value of T, is the classical reduced modulus load, in agreement with existing stability criteria for rate-independent models based on maximum dissipation. For arbitrary values of T, two critical loads are identified at the linear stability transition. The first is named the rate-dependent tangent modulus load and is valid for perturbations sufficiently small to prevent initial unloading. That load coincides with the classical tangent modulus load for T tending to zero and is, surprisingly, a decreasing function of that dimensionless number. The second critical load is termed the rate-dependent reduced modulus load, and is applicable to columns that are partly unloaded at the onset of perturbation. This critical load approaches the classical reduced modulus load in the limit of T tending to zero, is a decreasing function of T, and depends on the imperfection size. Similar results are found for the second model, with a new insight on the role of the unloading zone extent in determining the critical load in the singular limit of T equal to zero. The proposed stability criterion is validated by comparing its predictions with the outcome of nonlinear perturbation analyses and of imperfection sensitivity studies. It is shown, in particular, that an imperfection evolves according to our stability predictions as

* Corresponding author

long as the relative difference between the irreversible displacements of the supports can be disregarded. A generalization of the proposed linear stability criterion to viscoplastic continua is finally sketched.

Keywords: Bucking; Structures; Beams and columns; Elastic–viscoplastic material; Stability and bifurcation

1. Introduction

It is proposed to capture the initial development of structural instabilities in strain-rate sensitive, dissipative solids and structures with the help of a stability criterion which accounts for the non-autonomous character of the governing equations. This new linear stability criterion is validated with the help of two structural models which are similar to Shanley's column (Shanley, 1947). The first model has discrete and the second model has continuously distributed elastic–viscoplastic supports. The generalization of the proposed stability criterion to continua, which is also sketched here, is the subject of forthcoming work.

The most frequently used model for the investigation of buckling in metallic structures subjected to quasi-static loading is the column under axial compression. The early works of Engesser (1889), Considère (1891) and Von Kàrmàn (1910) established the load at which an axially compressed column becomes unstable. Shanley (1947) was the first to explain, by using a simple model and experimental verifications, that the tangent modulus load of Engesser (1889) is the lowest load at which the axially compressed column starts deflecting laterally. At the same time Von Kàrmàn (1947) pointed out that the first bifurcation is under increasing load and is, in this sense, stable and that the perfect column's stability is lost at a larger load termed the reduced modulus load. Duberg and Wilder (1952) included initial imperfections in their study of the post-buckling range to show how the tangent modulus load approximates the maximum load bearing capacity of real structures.

The generalization of the bifurcation criterion to arbitrary rate-independent elasto-plastic solids is due to Hill (1956, 1958), who used the same mathematical framework to include buckling, necking and localization phenomena. He gave sufficient conditions for the exclusion of bifurcation in the incremental (rate-one) problem of an elastoplastic solid and conjectured that these conditions should also guarantee uniqueness. Hill also investigated the condition for stability in elasto-plastic problems by means of calculating the dissipation produced by small perturbations about the state in question. He showed that his criterion for the exclusion of rate-one bifurcation was also sufficient for the stability in the sense of positive dissipation. Similar problems were also studied by Nguyen and Radenkovic (1975) and subsequently by Nguyen (1984) who discussed the difference between onset of bifurcation and instability for a general class of solids that obey the maximum dissipation principle. In addition, the works of Hutchinson (1973a,b, 1974) established a general method for calculating the post-bifurcation behavior and the imperfection sensitivity of rate-independent solids, as a basis to predict their maximum load carrying capacity.

Despite the significant progress in our comprehension of instability problems in rate-independent elasto-plastic structures, two inadequacies of the existing theoretical framework remain. The first pertains to the class of constitutive laws admissible by the existing general theory which has been developed for materials obeying the maximum dissipation principle, i.e. the normality of plastic flow to the current yield surface. This theoretical restriction gives rise to self-adjoint problems and consequently excludes the study of frictional systems (see discussion in Triantafyllidis and Leroy, 1994). The second inadequacy, of interest to this paper, pertains to the need of introducing strain-rate dependency to explain certain instability phenomena. For example, it is known that minute amounts of strain-rate sensitivity have significant effects in the stability predictions of strained solids, such as the delay of necking in axially stretched bars (Hutchinson and Neale, 1977). For some micromechanical slip-based models of metal plasticity (Asaro, 1983) the inclusion of rate-dependency effects removes the non-uniqueness in the response of the rate-independent model with important implications on the stability of crystals (Pan and Rice, 1983). The above mentioned instabilities of rate-dependent solids cannot be detected by a bifurcation analysis which, if based on the instantaneous material response, predicts an Euler-type of load (Mandel, 1971). Arguments based on dissipation at the neighborhood of an equilibrium (Nguyen and Radenkovic, 1975) do not account for the time evolution of the fundamental solution and thus can only provide partial information on stability. It is therefore necessary to follow the evolution of a perturbation away from the *time-dependent* solution whose stability is under investigation.

The lack of a general theory for the stability of rate-dependent solids has resulted in the proposition of various stability criteria and methods of investigation for specific applications. One approach, which extends the work of Hutchinson (1974), consists of following the development of an initial imperfection in the rate-dependent system (Tvergaard, 1985). Such analyses often require numerical solutions and provide the maximum bearing capacity of the structure which is the relevant information for design. However, the debate remains open on how to complement those nonlinear numerical calculations by simpler analytical methods which make use of our knowledge of the fundamental solution, to provide information on the initial evolution of small imperfections. The simplest method proposed so far estimates the slope of the stress–strain relation and uses the resulting moduli in a bifurcation analysis (Bodner et al., 1991) as it was already suggested by Carlson (1956) to extend the results of Shanley (1947) to creep buckling problems. Note that such approximations should not be compared with maximum load estimates, as pointed out again recently by Mikkelsen (1993), due to the delay in the instability development discussed above. An alternative approach is to conduct a linear perturbation analysis which results in a system of differential equations with time-dependent coefficients, frequently discontinuous functions of position due to the presence of unloading. A simplified solution to these non-autonomous systems of governing equations is obtained with the so-called frozen coefficient approximation. It consists of ignoring the time-dependence of the coefficients and thus, physically, to consider only perturbations with a rapid growth compared to the fundamental solution evolution. Such approximations have been applied successfully to various problems, including the detection of the

onset of adiabatic shear bands (Clifton, 1978; Anand et al., 1987), and often permit the derivation of elegant analytical solutions. The merits of the frozen coefficient assumption for structural problems were recognized by Leroy (1991) who also showed that the resulting stability predictions collapse to Shanley's tangent modulus load or to Hill's bifurcation criterion in the limit of inviscid plasticity. Despite these useful results, the mathematical inadequacy of the frozen-coefficient approximation remains: it should not be employed close to the stability threshold since the perturbation rate of growth is then comparable to the evolution of the fundamental solution.

The objective of this paper is to propose a linear stability criterion based on the investigation of the linearized system at the onset of perturbation which correctly accounts for the time-dependence of the fundamental solution and thus should overcome the shortcomings of the frozen coefficient approximation. More specifically, for the two structural problems considered, it is found that it is the change in sign of the second time derivative of the angular position of the column structure which signals the onset of instability. The load corresponding to this transition is termed the critical load. Two time scales are explicitly introduced corresponding to the relaxation time of the viscous material and the characteristic time of loading. The critical loads depend on the ratio T of these two characteristic times and on the size of the initial perturbation of the system. Although the proposed stability criterion is introduced and validated with the help of the two Shanley-type models, the ideas can be generalized to continua, as it is briefly discussed at the end. It is emphasized that the linear stability criterion proposed is not aimed to capture the long-term evolution of the perturbations. The non-linear results show how the verdict of our criterion could be altered or confirmed in the long term depending on geometrical properties and boundary conditions.

The contents of this paper are as follows. The next section presents the two structural models considered and their equilibrium solutions obtained for T equal to zero. Section 3 pertains to the application of our linear stability criterion for the discrete structural model. It is found that the critical load for principal equilibria, defined for a straight column and T equal to zero, is the classical reduced modulus load for rate-independent models, as expected from existing stability criteria based on maximum dissipation (Nguyen and Radenkovic, 1975). For arbitrary values of T, two critical loads are defined. The first is termed the rate-dependent tangent modulus load and results from perturbations that are small enough to exclude unloading. That load is a decreasing function of T and tends to the classical tangent modulus load as T approaches zero. The second critical load is termed the rate-dependent reduced modulus load, and is applicable to columns that exhibit unloading at the onset of perturbation. This critical load is also a decreasing function of T, depends on the imperfection size and tends to the classical reduced modulus load in the limit of T approaching zero. Results reported in the main text are for a force control set-up, while those for displacement control are discussed in the Appendix. Section 4 contains the extension of those findings to the second model which has a continuous distribution of support. The sensitivity of the critical load's singular limit, as T approaches zero, to the size of the unloading zone at the onset is explored. The extension of the linear stability criterion to elastic–viscoplastic solids is finally sketched

in Section 5. The reader will find preliminary results on this generalization in Triantafyllidis et al. (1997).

2. The two structural examples and their equilibrium solutions

The two structural problems chosen to motivate a stability criterion which can be generalized to viscoplastic solids are now presented. For reasons of completeness, we also review in this section their equilibrium solutions which are independent of time. Both the force and the displacement formulation are considered in this paper but the details of the analysis for the second formulation are postponed to the Appendix.

The study of the Shanley column has long been the example of choice for explaining the stability of more complicated elasto–plastic structures and has thus been frequently used in the literature on plastic buckling. It was introduced by Shanley (1947), as a simplified model for the compressive buckling of an I beam (the two inelastic supports idealize the outer flanges of the I beam). Hutchinson (1973a, b) generalized it by introducing continuously distributed support and a lateral spring, the latter to simulate the geometric and material nonlinearities present in more realistic structures. It is the Shanley column with discrete supports and a lateral spring which constitutes our first example while the second deals with the same structure except for a continuous distribution of support. This refinement is necessary to relate the extent of the unloading zone to the bifurcation load.

2.1. *First model*: *discrete supports*

The planar model, which is depicted in Fig. 1(a), consists of a horizontal bar of length $2l$ attached to a vertical bar of length L. The bar and the connection are rigid. The system has two degrees-of-freedom, the vertical displacement v of the connection point of the two bars and the rotation θ of the structure about the same point, Fig. 1(b). It is assumed throughout this paper that the value of θ is small compared to unity and also, due to symmetry, constrained to be always positive. The structure is attached to two identical inelastic supports, labeled 1 and 2 and drawn as springs in Fig. 1(a), at the ends of the horizontal bar. In addition, a nonlinear elastic spring, labeled 3, is attached to the top of the vertical bar. A force P is applied vertically to the structure and it is balanced by the two vertical reactions F_1 and F_2 provided by the inelastic supports, as shown in the free-body diagram of Fig. 1(b). The horizontal reaction F_3 of the nonlinear elastic spring is defined as $k\theta^3$ with k a constant. The fundamental equilibrium solutions and trajectories of the problem correspond to a straight column that remains untilted. The stability of equilibria or of trajectories is examined by applying a moment $\tilde{m}$ which is kept constant in time after perturbation, Fig. 1(b). That moment is applied as soon as the loading is initiated if an imperfection analysis is conducted.

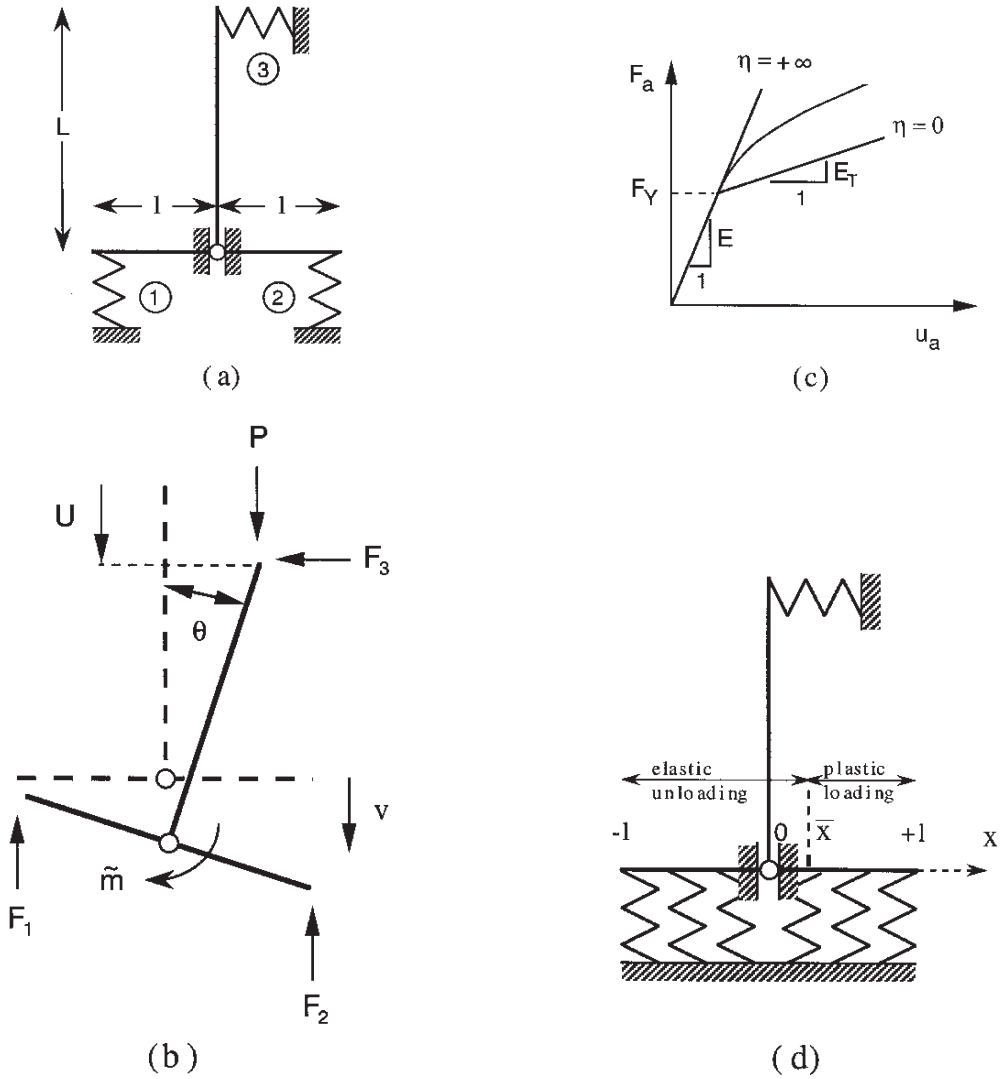

Fig. 1. The two structural examples considered correspond to Shanley's column with discrete and a continuous distribution of viscoplastic supports. The first model with discrete supports and its free-body diagram are shown in (a) and (b). The response of each support is presented in (c). The second model with a continuous support is shown in (d).

2.1.1. *Governing equations*

The equilibrium of force and moment provide explicit expressions for the two forces F_a[1]

$$F_a = \frac{1}{2}\left[P \mp \frac{L}{l}(P\theta - k\theta^3) \mp \frac{\tilde{m}}{l}\right]. \tag{2.1}$$

[1] Here and subsequently, a variable followed by a Latin subscript ($a = 1, 2$) designates its association to the corresponding inelastic support. Furthermore, if two signs appear simultaneously, as in (2.1), the upper sign is for support 1 and the lower for support 2.

In view of the small-rotation assumption, the work-conjugate displacements u_a to the forces F_a are

$$u_a = v \mp l\theta. \tag{2.2}$$

The vertical displacement U of the point of application of the force P is

$$U = v + \frac{L}{2}\theta^2. \tag{2.3}$$

The displacement u_a of each inelastic support is decomposed into an elastic part u_a^{e} proportional to the force F_a by a constant E[2] and an inelastic part u_a^{p} which define the two internal variables of the system

$$u_a = u_a^{\mathrm{e}} + u_a^{\mathrm{p}} \quad \text{with} \quad u_a^{\mathrm{e}} = F_a/E. \tag{2.4}$$

The linear elasto-viscoplastic model of Malvern (1951) is chosen, in view of its relative simplicity, to govern the evolution of the two internal variables:

$$\dot{u}_a^{\mathrm{p}} = \begin{cases} (F_a - F_a^{\mathrm{p}})/\eta & \text{if} \quad F_a > F_a^{\mathrm{p}} \\ 0 & \text{if} \quad F_a \leqslant F_a^{\mathrm{p}} \end{cases}, \tag{2.5}$$

where F_a^{p}, the current force necessary for support a to yield, is assumed to be a linear function of the internal variable u_a^{p}

$$F_a^{\mathrm{p}} = F_{\mathrm{Y}}(1 + h u_a^{\mathrm{p}}). \tag{2.6}$$

The coefficient h in (2.6) is the hardening parameter and the constant F_{Y} the initial yield force. A typical force F_a vs displacement u_a response for the elasto-viscoplastic supports is depicted in Fig. 1(c). As the viscosity parameter η tends to zero, the response collapses to its rate-independent counterpart while for η tending towards infinity, the behavior approaches the response of a linear elastic solid. The slope of the rate-independent curve in the inelastic range is the tangent modulus: $E_{\mathrm{T}} = E/(1 + E/F_{\mathrm{Y}}h)$. The time-independent response varies from elastic–perfectly plastic to linearly elastic, as h is chosen from 0 to infinity.

At this point we introduce the two time scales of the problem starting with the relaxation time t_r of the column support and the associated dimensionless time τ:

$$t_{\mathrm{r}} \equiv \eta/F_{\mathrm{Y}}h, \quad \tau \equiv t/t_{\mathrm{r}}. \tag{2.7}$$

Note that a superposed dot denotes the derivative with respect to the physical time t while derivatives with respect to τ are denoted either by $\mathrm{d}(\,)/\mathrm{d}\tau$ or by $(\,)_{,\tau}$. The second characteristic time of the problem t_{l} is associated to the rate of applied loading ($\dot{P} = V$ for force control) and is defined by $t_{\mathrm{l}} \equiv F_{\mathrm{Y}}/V$. The presence of two time scales leads to the introduction of a dimensionless number T defined as the ratio of the relaxation time over the characteristic loading time

[2] Termed the '*elastic modulus*' but having dimension of force over length.

$$T \equiv \frac{t_r}{t_1} = \frac{V\eta}{F_Y^2 h}. \tag{2.8}$$

The same notation V is used in the Appendix for displacement control ($\dot{U} = V$) resulting in a single definition of T.

2.1.2. *Equilibrium solutions*

We now turn our attention to a description of the equilibrium solutions. Equilibrium is characterized by either a zero relaxation time or an infinite loading time and in both cases $T = 0$. In that instance, the viscosity relation (2.5) provides a yield criterion for the rate-independent model. The set of equilibrium solutions is parameterized in two ways depending on the value of the tilt angle. First, the applied force P is used for the fundamental solution ($\theta = 0$) as a monotonically increasing function which replaces the physical time t. Second, any bifurcated equilibrium path ($\theta \neq 0$) is parameterized by the angular position θ which is then the time-like parameter. With this parameterization, the rate $\dot{u}_a^p$ of the internal variable is well defined along any equilibrium path and is constrained by

$$\dot{u}_a^p \begin{cases} > 0 & \text{if} \quad F_a = F_a^p \\ = 0 & \text{if} \quad F_a < F_a^p \end{cases}. \tag{2.9}$$

Combination of the displacement decomposition in (2.4) with the equilibrium equations (2.1) and the kinematic relations (2.2.) provides the following expression for the internal variables

$$u_a^p = v \mp l\theta + \frac{1}{2E}\left[-P \pm \frac{L}{l}(P\theta - k\theta^3) \pm \frac{\tilde{m}}{l} \right]. \tag{2.10}$$

Note that this expression is also valid for arbitrary values of T. From the equilibrium equations (2.1) and the constitutive equations (2.4) and (2.6) applied to the principal solution in the plastic range ($P > P_Y \equiv 2F_Y$), the forces, displacements and internal variables of the model are found in terms of the prescribed force P to be

$$\begin{aligned} F_a^0 &= \frac{P}{2}, \\ (u_a^p)_0 &= \left[\frac{P}{2F_Y} - 1 \right] \frac{1}{h}, \\ v_0 &= \frac{P}{2E}\left[1 + \frac{E}{F_Y h} \right] - \frac{1}{h}. \end{aligned} \tag{2.11}$$

The zero in subscript or superscript in (2.11) and in what follows is reserved for quantities evaluated along the fundamental equilibrium solution. As the applied force P increases along the principal path, the following characteristic forces are reached successively:

$$P_Y \equiv 2F_Y,$$
$$P_T \equiv P_E/[1+E/F_Y h],$$
$$P_R \equiv P_E/[1+E/2F_Y h],$$
$$P_E \equiv 2El^2/L, \tag{2.12}$$

in which P_Y is the force necessary to initiate yield and P_E is the Euler load. The interpretation of the tangent modulus and reduced modulus load P_T and P_R are provided in the bifurcation analysis which follows.

At bifurcation ($\theta \neq 0$), the rate form of the equilibrium equations (2.1) combined with the rate-independent loading and unloading conditions (2.9) reveals that $\dot{F}_1$ is negative or zero and $\dot{F}_2$ positive or zero. Bifurcation is characterized by an elastic unloading of support 1 ($\dot{F}_1 < 0$) if the applied load P_0 is larger than P_T and by neutral loading ($\dot{F}_1 = 0$) at the load P_T. The '*tangent modulus load*' P_T introduced by Engesser (1889) is the lowest possible force at which a bifurcation from the principal branch occurs. This terminology is due to the fact that P_T is the critical force found in a rate-one bifurcation analysis if the two supports' response is given by the tangent modulus E_T. Similarly, the loading condition of support 2 requires the applied load P_0 to be strictly less than P_E and neutral loading of that same support is met exactly at P_E.

Leaving aside the neutral conditions met at P_E and P_T for θ equal to zero, we adopt in what follows the unloading condition for support 1 and loading condition of support 2 for all non-zero values of θ. These conditions are met for all results to be reported in this section. They are now combined with the equilibrium equations (2.1) and the hardening law (2.6) for support 2 and result in the following P–θ relation for all equilibrium paths intersecting the fundamental solution at P_0:

$$P = \frac{P_0 + (4F_Y hl\theta/P_R)(P_R + k\theta^2)}{1+(4F_Y hl\theta/P_R)}. \tag{2.13}$$

The bifurcation diagram obtained from (2.13) is a one-parameter (θ) family of paths emerging from any point P_0 on the principal branch between P_T and P_E, as depicted by the continuous lines in Fig. 2 for three different values of the nonlinear spring stiffness k. Note that all graphs presented here are constructed with the following values of the dimensionless geometric and material parameters: $L/l = 25$, $F_Y h/E = 0.1$ and $hl = 40$. For the sake of clarity, the characteristic loads P_T, P_R and P_E are indicated on the force axis by the letters 'T', 'R' and 'E', respectively, in Fig. 2 as well as in the other figures of the paper. The initial slope $(\mathrm{d}P/\mathrm{d}\theta)_0$ of the bifurcated equilibrium paths is positive for load between P_T and P_R and negative between P_R and P_E as illustrated in Fig. 2(c). The '*reduced modulus load*' P_R is the bifurcation load at which the instantaneous responses of the second and first supports are given by E_T and E, respectively. Notice also that the bifurcated equilibrium path through P_R is the limit towards which all the bifurcated equilibrium paths converge for large values of the rotation angle θ. In the absence of the nonlinear spring 3, the equilibrium path emerging from P_R is independent of θ, as seen in Fig. 2(a). For positive and negative stiffness of the nonlinear spring 3, the load corresponding to the bifurcated

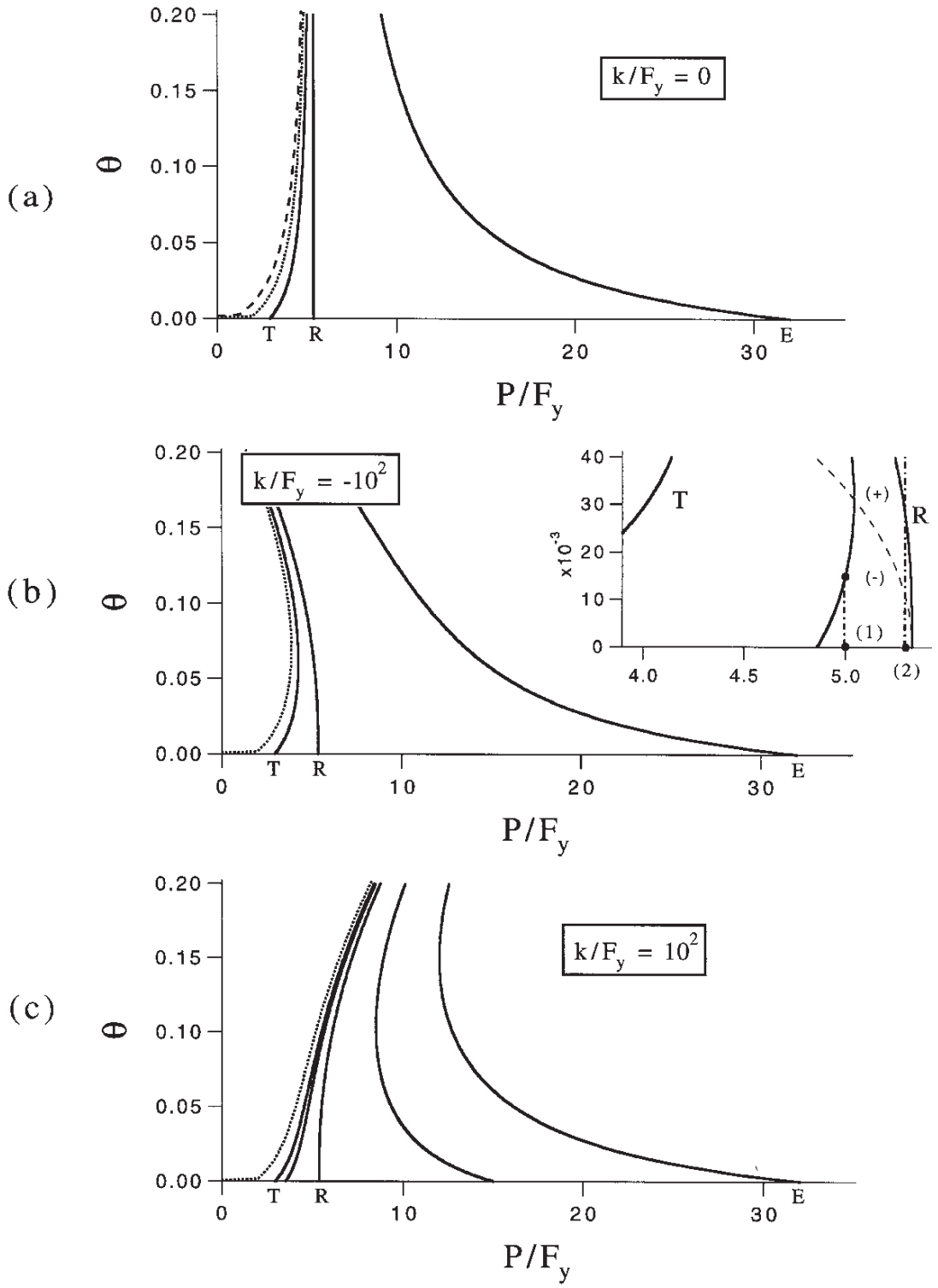

Fig. 2. Equilibrium solutions in a space spanned by the column's angular position and normalized applied force for the discrete model and three different values of the nonlinear spring stiffness. Any point on the principal equilibrium branch ($\theta = 0$) between the tangent modulus load (marked by T) and the Euler buckling load (marked by E) is a bifurcation point. The bifurcated equilibrium branches through the reduced modulus load (marked by R) intersect the principal branch at a right angle. The dashed and dotted curves correspond to the equilibrium path of an imperfect model with θ^* equal to 10^{-3} and 10^{-4}, respectively. The dashed curve in the insert of (b) connects the extrema of all equilibrium paths and partitions the space in stable and unstable regions, in the dissipation sense, marked by a minus and a plus sign, respectively.

path through P_R is a decreasing (Fig. 2(b)) and an increasing (Fig. 2(c)) function of θ, respectively.

The rest of this subsection is devoted to the response of imperfect columns, modeled by the application of a constant moment $\tilde{m}$. Such imperfections are inevitable in the physical realization of the column which does not follow the principal nor the bifurcated equilibrium paths discussed above. The imperfect structure follows a unique equilibrium path whose expression is not presented here for sake of conciseness. The imperfect structure has initially an angle θ^* at P equal to zero due to application of $\tilde{m}$. For a small enough initial angle, the structure responds elastically and the initial angular position is related to the applied moment by $\theta^* = \tilde{m}/2El^2$. As loading proceeds, θ increases from θ^* and both elastoplastic supports undergo plastic deformation. Then, support 1 unloads elastically while support 2 continues to load plastically. Results are depicted by dotted and dashed curves in Fig. 2 for an initial angle of 10^{-4} and 10^{-3}, respectively. As the size of the imperfection tends to zero, the equilibrium curves tend to the equilibrium solution of the perfect structure which emerges from P_T, as can be concluded from Fig. 2(a). These results are typical of any imperfect rate-independent elastoplastic structure whose perfect counterpart has a simple bifurcation eigenmode (Hutchinson 1973a, b, 1974).

2.2. *Second model*: *continuous support*

This second model with a continuous distribution of supports is essential to illustrate the connection between the load at the emergence of a bifurcated equilibrium path and the size of the initial elastic unloading zone. A schematic representation of the continuous support version of the rigid T model is given in Fig. 1(d). The force and moment equilibrium equations for this second model are

$$\int_{-l}^{l} F(x)\,\mathrm{d}x = P,$$

$$\int_{-l}^{l} xF(x)\,\mathrm{d}x = PL\theta - kL\theta^3, \tag{2.14}$$

where x is the position coordinate attached to the bar of length $2l$, Fig. 1(d). From kinematics, the displacement $u(x)$, work-conjugate to the force per unit length $F(x)$ of the continuous support, is

$$u(x) = v + x\theta, \tag{2.15}$$

while the displacement U at the point of application and in the direction of the force P is still given by (2.3). The constitutive equations for the rate-independent elastoplastic supports are still (2.4)–(2.6) in which the discrete quantities u_a, u_a^e, u_a^p, F_a and F_a^p are now replaced by their continuous counterparts $u(x)$, $u^e(x)$, $u^p(x)$, $F(x)$, and $F^p(x)$, respectively.

We now concentrate on the new information of this second model which is the one-to-one correspondence between every bifurcated equilibrium path and the initial size of the elastic unloading zone. The time-like parameterization of the equilibrium

equations is similar to the one discussed for the first model. The rate form of the equilibrium and constitutive equations is necessary to characterize the initial conditions on the bifurcated equilibrium paths. Assuming that at a given stage of deformation the elastic unloading zone is $[-l, \bar{x}]$, the rate form of the equilibrium equations (2.14) yields, with the help of the constitutive law (2.4)–(2.6),

$$\int_{-l}^{\bar{x}} E(\dot{v}+x\dot{\theta})\,\mathrm{d}x+\int_{\bar{x}}^{l} E_{\mathrm{T}}(\dot{v}+x\dot{\theta})\,\mathrm{d}x=\dot{P},$$

$$\int_{-l}^{\bar{x}} E(\dot{v}+x\dot{\theta})x\,\mathrm{d}x+\int_{\bar{x}}^{l} E_{\mathrm{T}}(\dot{v}+x\dot{\theta})x\,\mathrm{d}x=\dot{P}L\theta+PL\dot{\theta}+3k\dot{\theta}\theta^{2}. \tag{2.16}$$

The boundary between the elastic and plastic loading zones $\bar{x}$ is a point of neutral loading found from the requirement $\dot{u}(\bar{x})=0$ which, from the kinematic relation (2.15), implies

$$\bar{x}=-\dot{v}/\dot{\theta}, \tag{2.17}$$

since for elastic unloading and plastic loading $\dot{u}(x)$ is strictly negative and positive, respectively.

We are now in a position to establish the relationship between bifurcation load and extent of the unloading zone. From the equilibrium equations (2.14)–(2.15) and their rate form in (2.16) applied at bifurcation ($\theta=0$) we obtain

$$\left(\frac{\mathrm{d}P}{\mathrm{d}\theta}\right)_{0}=-\frac{1}{2}(E-E_{\mathrm{T}})(\bar{x}_{0})^{2}-(E+E_{\mathrm{T}})l\bar{x}_{0}-\frac{1}{2}(E-E_{\mathrm{T}})l^{2},$$

$$P_{0}L=-\frac{1}{6}(E-E_{\mathrm{T}})(\bar{x}_{0})^{3}+\frac{1}{2}(E-E_{\mathrm{T}})l^{2}\bar{x}_{0}+\frac{1}{3}(E+E_{\mathrm{T}})l^{3}. \tag{2.18}$$

The second of these two equations reveals that for $\bar{x}_0$ equal to $-l$ the entire structure loads plastically, except for the neutral loading at $-l$, and, consequently, the bifurcated equilibrium branch emerges from the fundamental solution at the tangent modulus load P_{T}. For $\bar{x}_0$ equal to l, the entire structure responds elastically, except for neutral loading at $+l$, and the bifurcated equilibrium branch originates from the fundamental solution at the Euler load P_{E}. Between these two extreme cases, the position of the unloading zone boundary $\bar{x}_0$ is a monotonically increasing function of the applied load P_0 in the interval $[-l, +l]$. The expressions for the main bifurcation loads for the continuous support model differ from their discrete counterparts defined in (2.12) and are given by

$$P_{\mathrm{T}}=\frac{P_{\mathrm{E}}}{1+E/F_{\mathrm{Y}}h},\qquad \bar{x}_{0}/l=-1,$$

$$P_{\mathrm{R}}=-P_{\mathrm{E}}\frac{4F_{\mathrm{Y}}h}{E}\frac{\bar{x}_{0}}{l},\quad \bar{x}_{0}/l=-(1+2F_{\mathrm{Y}}h/E)+[(1+2F_{\mathrm{Y}}h/E)^{2}-1]^{1/2},$$

$$P_{R'} = P_E \frac{1+E/(2F_Y h)}{1+E/(F_Y h)}, \quad \bar{x}_0/l = 0,$$

$$P_E = \frac{2El^3}{3L}, \qquad \bar{x}_0/l = +1. \tag{2.19}$$

The reduced modulus load for force control denoted by P_R has the same definition as in the first model. Note the introduction of a second reduced modulus load $P_{R'}$ which is obtained for the displacement boundary condition ($dU/d\theta = 0$). These critical loads P_R and $P_{R'}$ are not associated with the same extent of the unloading zone. The bifurcation diagram of the second model is qualitatively similar to the ones depicted in Fig. 2 and is not presented here for sake of conciseness. An infinity of equilibrium paths emerge from the principal branch between P_T and P_E and the size of the unloading zone is related to P_0 according to $(2.18)_2$. As for the column with discrete support, it can be shown from $(2.18)_1$, that the slope $(dP/d\theta)_0$ is positive and negative for P_0 between P_T and P_R and between P_R and P_E, respectively.

3. Stability of a Shanley column with discrete supports

In this section, we investigate the stability of principal equilibria ($T = 0$) and principal trajectories ($T \neq 0$) and propose a stability criterion based on the linearized governing equations of the discrete support model. To explore the validity of this criterion, its predictions are compared with the numerical solution of the nonlinear evolution of the perturbed system. Linear and nonlinear stability predictions are finally compared with the results of an imperfection sensitivity study to define the conditions for which stability and imperfection analyses provide similar results. Only the case of force control is examined here and the different stability predictions for displacement control are postponed to the Appendix.

3.1. *Initial conditions for the linear stability problem*

To initiate the calculations for a perturbed column we must determine all variables at time t^* referred to as the onset of perturbation. The perturbed state of the structure at time t^* results from the application during the time interval $[t^* - \Delta t, t^*]$ of a moment $\tilde{m}$ which increases smoothly over that time period to reach a value which is kept constant thereafter. The time interval Δt is assumed to be small compared to the two time scales of the evolution problem. Let $\tilde{f}$ denote the difference between the perturbed and fundamental values of any quantity f at the onset of perturbation, i.e. $\tilde{f} \equiv f(t^*) - f_0(t^*)$. From the viscosity law (2.6), the perturbation $\tilde{u}_a^{p*}$[3] is found to be

[3] Here and subsequently a symbol followed by a * in superscript signals that the quantity of interest is evaluated at the onset of perturbation.

$$\tilde{u}_a^{p*} = \int_{t^*-\Delta t}^{t^*} \dot{\tilde{u}}_a^{p}\,\mathrm{d}t = \frac{\Delta t}{\eta}\frac{\tilde{F}_a^*}{2} + \mathcal{O}\left[\left(\frac{\Delta t}{\eta}\right)^2\right]. \tag{3.1}$$

This quantity can be disregarded compared to the elastic perturbation $\tilde{u}_a^{e}*$, which is equal to $\tilde{F}_a^*$, if the time interval Δt is small compared to η/E. The perturbation of the internal variables at the onset is thus negligible compared to the perturbed elastic displacement and the initial response of the system is, to first order, purely elastic. Consequently, the details of the perturbation path during $[t^*-\Delta t, t^*]$ are unimportant.

From the linearized version of the governing equations (2.1)–(2.5), one obtains for the perturbations in applied load and moment

$$\tilde{P}^* = 2E\tilde{v}^*, \quad \tilde{m} = (P_E - P_0)L\tilde{\theta}^*. \tag{3.2}$$

For a force controlled test, the perturbation $\tilde{P}$ must be zero and hence the initial displacement perturbation $\tilde{v}^*$ is also zero. Conversely, for a displacement control and according to (2.3), $\tilde{v}^*$ is equal to $\tilde{U}$ which is zero and the initial perturbation in applied force $\tilde{P}^*$ is thus also zero following (3.2). Furthermore, from the second equation in (3.2), we find that the perturbation by a constant moment $\tilde{m}$ implies an equivalent initial perturbation of the angular position θ^*. To summarize, the linearized initial perturbations of the forces, displacements and internal variables of the model are independent of the type of loading and are related at the onset by

$$\begin{aligned} &\tilde{u}_1^{p*} = \tilde{u}_2^{p*} = 0, \quad \tilde{u}_1^{e*} = -l\theta^*, \quad \tilde{u}_2^{e*} = l\theta^*, \\ &\tilde{P}^* = 0, \quad \tilde{U}^* = 0; \quad \tilde{v}^* = 0, \quad \tilde{\theta}^* = \tilde{m}/L(P_E - P_0). \end{aligned} \tag{3.3}$$

These results constitute the initial conditions for the stability analysis which are considered in the next two subsections, first, for T equal to zero and, second, for arbitrary values of T.

3.1.1. *Linear and nonlinear stability of the principal equilibrium path* (T = 0)

The stability investigation of the principal equilibrium path under force control starts with the presentation of the nonlinear governing equations. Subsequently, a linear stability criterion is proposed, based on the initial response of the linearized version of these equations. Note that the initial conditions discussed above are valid since T is set to zero by selecting a finite value of the relaxation time t_r and setting the characteristic loading time t_l to infinity. The second choice which consists of selecting a zero viscosity and a finite loading rate is not acceptable since it would render the column's constitutive response rate-independent and stability should then be discussed within the framework proposed by Nguyen (1984). In the final part of this section, the numerical solutions of the nonlinear governing equations are employed to check the validity of the linear stability criterion. Time at the onset is set to zero for simplicity.

As a preliminary to the set up of the governing equations for the tilted column, we first consider the loading conditions of the two supports. By combining the principal solution (2.11) with the equilibrium equations (2.1) and the initial perturbation relations in (3.3), we see that support 1 unloads elastically while support 2 loads

plastically at the onset. Assuming that those conditions are maintained (a fact which is verified a posteriori) one obtains the following governing equation

$$v-l\theta+\frac{1}{2E}\left[-P_0+\frac{L}{l}\left(P_0\theta-k\theta^3\right)+\frac{\tilde{m}}{l}\right]=\left[\frac{P_0}{2F_Y}-1\right]\frac{1}{h}. \tag{3.4}$$

The viscosity law (2.5) for the second support is now combined with the equilibrium equations (2.1), the internal variable relations in (2.10) and the dimensionless time definition in (2.7) to provide

$$\frac{\mathrm{d}}{\mathrm{d}\tau}\left[P_0\theta-k\theta^3\right]+\left[P_0\theta-k\theta^3+\frac{\tilde{m}}{L}\right]\left[1+\frac{E}{2F_Yh}\right]=\frac{2El^2}{L}\left[\frac{\mathrm{d}\theta}{\mathrm{d}\tau}+\theta\right]. \tag{3.5}$$

The above two nonlinear governing equations are complemented by the following initial conditions which are derived by combining the principal equilibrium (2.11) and the initial perturbation relations (3.3)

$$v^*=\frac{P_0}{2E}\left[1+\frac{E}{F_Yh}\right]-\frac{1}{h},\quad u_a^{p^*}=\left[\frac{P_0}{2F_Y}-1\right]\frac{1}{h}. \tag{3.6}$$

The loading conditions of the two supports provide the inequality

$$\left[\frac{L}{l}\left(P_0\theta-k\theta^3\right)+\frac{\tilde{m}}{l}\right]\left[1+\frac{2F_Yh}{E}\right]>4F_Yhl\theta, \tag{3.7}$$

which is automatically satisfied at the onset τ^*. The nonlinear equations (3.4)–(3.5), the constraint (3.7) and the initial conditions (3.6) are the equations governing the evolution of an initial perturbation from the principal equilibrium state.

The stability criterion is now presented. It is based on the initial behavior of the linearized version of the above nonlinear governing equations. The imposed initial conditions (3.6) in conjunction with the initial perturbation relations (3.3) and the linearized version of (3.5) determine the initial rate of θ to be

$$\left(\frac{\mathrm{d}\theta}{\mathrm{d}\tau}\right)^*=\frac{E\theta^*}{2F_Yh}\frac{1}{1-P_0/P_E}. \tag{3.8}$$

This first result indicates that the rate of rotation is always positive since the perturbation in rotation θ^* is positive and the load P_0 at which the perturbation occurs is less than the Euler load P_E. The perturbation leads to an initial positive growth of the angle θ and the question raised is whether that growth will be maintained with time or will decrease at the approach of a new stable equilibrium state. To explore these two possibilities at the onset of the perturbation, our only means is to inspect the second derivative of θ with respect to τ at the onset.

From (3.5)–(3.6), (3.8) and the definitions for P_E, P_R in (2.12) we obtain upon linearization the following expression for this second derivative:

$$\left(\frac{\mathrm{d}^2\theta}{\mathrm{d}\tau^2}\right)^* = \frac{E\theta^*}{2F_Y h}\frac{P_0/P_R - 1}{(P_0/P_E - 1)^2}. \tag{3.9}$$

To interpret the above result, note that the denominator of the second fraction on the right-hand-side of (3.9) is always bounded and that the sign of the second derivative is governed by the numerator. The numerator is negative if the applied load is less than the reduced modulus load P_R, indicating that the positive rotation rate is decreasing just beyond the onset. A possible interpretation is that the rotation rate will decrease towards a zero value signalling that a new equilibrium is reached in the vicinity of the fundamental solution. To the contrary, if the applied load P_0 is larger than the reduced modulus load P_R, the numerator on the right-hand-side of (3.9) is positive, and the rotation rate increases, at least initially, beyond the onset. This interpretation of (3.9) is in line with the dissipation based result of Nguyen and Radenkovic (1975) and leads to the following stability criterion. *It is proposed to define a stable equilibrium as one for which the second time derivative of the perturbation in rotation is negative at the onset*.

In what follows, we first validate our proposition by comparing its predictions with the results of numerical simulations. Our criterion is extended to the case of arbitrary values of T in the next subsection. The solution procedure for the nonlinear stability analysis is achieved via a fourth-order Runge–Kutta scheme. The constant k of the nonlinear spring 3 is $-10^2 F_Y$ and corresponds to the value taken to draw the bifurcation equilibrium in Fig. 2(b). The nonlinear results of the perturbation problem under force control are depicted in Fig. 3. They correspond to the evolution of the rotation rate $\theta_{,\tau}$—normalized by the initial rate $|\theta^*_{,\tau}|$—as a function of the dimensionless time τ. The nonlinear results are depicted by solid lines and the linear stability predictions by dashed lines. In Fig. 3(a), results are calculated for an initial perturbation angle of 1.7×10^{-4} and for three different loads. The first two are below the reduced modulus load P_R and correspond to points 1 and 2 in the insert of Fig. 2(b), while the third load is larger than P_R. As expected from the linear stability predictions, the initial slope for a load less than P_R is negative and positive for a load larger than P_R. Note that for the latter case, the linear stability verdict is confirmed by the nonlinear analysis and the growth rate becomes unbounded with time.

The nonlinear results for loads less than P_R are more complex. For the lower load (point 1 in Fig. 2(b)), the rate of rotation decreases and tends to a zero value, as shown by the solid curve marked Case 1 in Fig. 3(a). The neighborhood of a new stable equilibrium which acts as an attractor is reached. This equilibrium is marked by a solid dot at the end of the dashed–dotted line starting from point (1) in Fig. 2(b). The equilibrium path emerging from the fundamental solution has also been drawn in the insert of Fig. 2(b) but we shall not try here to link the selection of that path to the amplitude of the perturbation applied. However, the case of larger load (point 2 in Fig. 2(b)) is different. The rate of rotation first decreases with time then increases without bound, as shown by the solid curve marked Case 2 in Fig. 3(a). To explain this nonlinear effect it is convenient first to define the dashed curve presented in the insert of Fig. 2(b). That curve is the parabola of equation $\theta^2 = (P - P_R)/3k$ obtained from (2.13), that intersects the locus of the maximum load

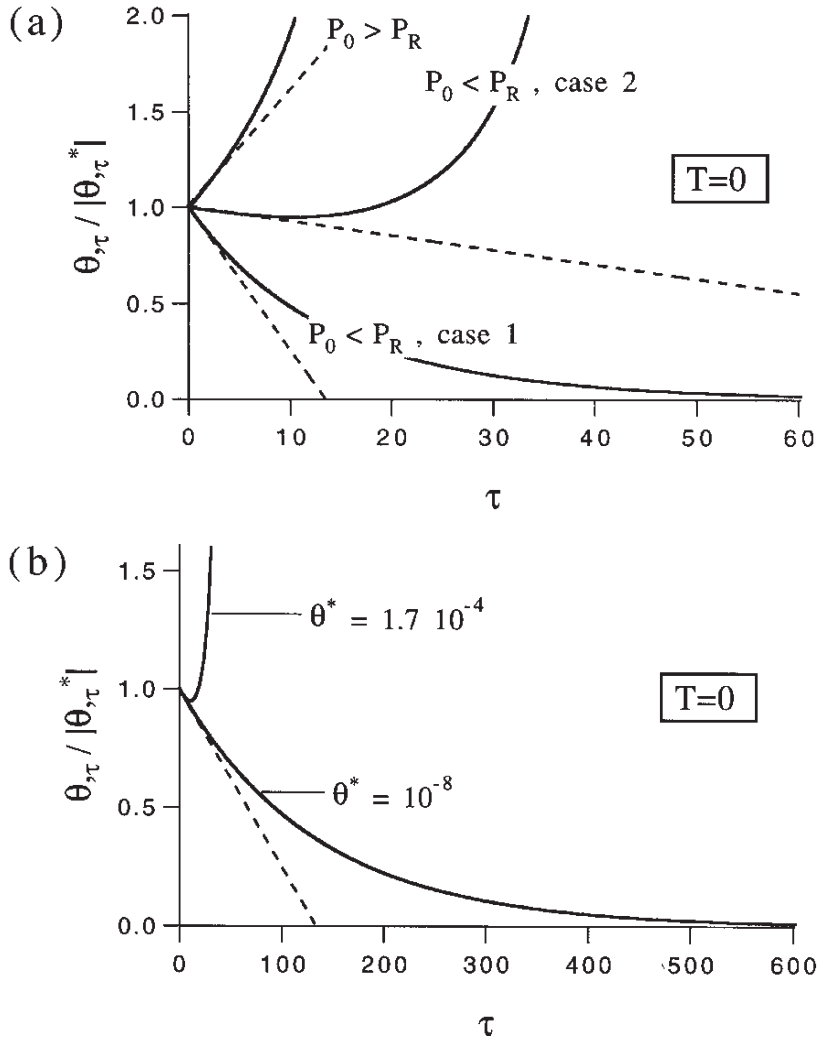

Fig. 3. The normalized rotation rate as a function of dimensionless time τ shows the evolution of a small perturbation from an equilibrium state for the rate-dependent discrete model under force control. In (a), results are obtained for three loads, two below the critical reduced modulus load. In (b), the influence of the perturbation size is shown for the intermediate load level which is slightly less than the reduced modulus load. The dotted lines correspond to the analytical solution of the linear stability criterion and the solid curves to the results of the nonlinear stability analysis. The bifurcation diagram of the rate-independent counterpart of the model is given in Fig. 2(b).

of all equilibrium paths for the tilted column. That curve partitions the space in two regions marked by a plus and minus sign. We state without proof that all equilibrium points in the region marked by the plus sign are unstable according to the dissipation criterion of Nguyen and Radenkowic (1975). Conversely, they are stable in the region marked by the minus sign. The nonlinear effect can now be explained as follows: as the rotation accumulates, the trajectory intersects the parabola and enters the region marked plus in which no stable equilibrium can act as an attractor. The rotation rate then increases without bound. To confirm this interpretation, results are presented in Fig. 3(b) for two initial perturbation sizes and for the same load marked 2 in Fig. 2(b). For the smaller perturbation size, the initial change in rotation rate is the same as the one reported for the larger perturbation size as well predicted by our criterion.

However, for the smaller perturbation size, the increase in angular position is not sufficient for the trajectory to intersect the parabola and a stable equilibrium can act as an attractor.

Rigorous proofs of these statements are not provided. This task is definitely beyond the scope of the present paper and is postponed to future work. The main conclusion here is that the nonlinear solution confirms the verdict of the linear stability analysis close to the principal equilibrium branch but that nonlinear effects could be sufficient to subsequently destabilize the column near the reduced modulus load depending on the perturbation size. Note that such effects are only possible for structures which have a strictly negative value for the stiffness of spring No. 3.

3.1.2. *Linear stability of principal trajectories* ($T \neq 0$)

It is now proposed to extend our stability criterion for arbitrary values of T. Following the derivation of an expression for the principal trajectories with constant force rate V, we present the nonlinear equations governing the evolution of a perturbation which is applied to that trajectory at time τ^*. It is shown that the stability of the principal trajectory depends on the size θ^* of the imposed perturbation relative to T, at a difference with the previous analysis. Indeed, two possibilities need to be distinguished, depending on whether or not the initial perturbation induces unloading of one of the two supports at the onset.

Choosing the origin of the dimensionless time ($\tau = 0$) to coincide with the first yield of supports, we define the applied load $P_0(\tau)$ as a function of the dimensionless number T

$$P_0(\tau) = F_Y(T\tau + 2). \tag{3.10}$$

For the principal solution of the perfect elasto-viscoplastic model, one obtains from (3.10) with the help of the internal variable equations (2.9) and (2.10) and the equilibrium equation (2.1)

$$\frac{dv_0}{d\tau} + v_0 = \frac{F_Y T}{2E}\left[1 + \tau(1 + E/F_Y h)\right] + \frac{F_Y}{E}, \tag{3.11}$$

to which the following initial condition must be added

$$v_0(0) = F_Y/E. \tag{3.12}$$

The solution of the above system (3.10)–(3.12) for the vertical displacement $v_0(\tau)$ is

$$v_0(\tau) = \frac{T}{2h}\left[\exp(-\tau) - 1 + \tau\right] + \frac{F_Y}{E}\left[1 + \frac{T\tau}{2}\right], \tag{3.13}$$

and defines, together with (3.10), the principal trajectory.

When the perturbation moment $\tilde{m}$ is applied to the structure at time τ^*, the relations between the initial perturbations of the various variables of the model are still given by (3.3). The only difference with the previous stability analysis of the principal equilibrium ($T = 0$) solution is that the initial loading or unloading condition for the inelastic supports 1 and 2 depends now on the size of the perturbation θ^* relative to

T. To establish the link between those two quantities, we combine the equilibrium equations (2.1), the relations for the internal variables and their rates (2.9)–(2.10) and the initial perturbation relations in (3.3) and obtain the following linearized expression for the rate of the two internal variables at the onset

$$(F_Y h)\left(\frac{\mathrm{d}u_a^p}{\mathrm{d}\tau}\right)^* = \mp El\theta^* + \frac{P_0^*}{2} - F_Y\left[1 + h\left(v_0^* - \frac{P_0^*}{2E}\right)\right]. \tag{3.14}$$

Using the principal trajectory information in (3.10), (3.13), we find from (3.14) that two cases have to be considered at the onset of perturbation:

$$\frac{\theta^*}{T} - \frac{F_Y}{2El}[1 - \exp(-\tau^*)] \begin{cases} < 0 \Rightarrow \text{supports 1 and 2 load} & \text{(Case I)} \\ > 0 \Rightarrow \text{support 1 unloads, 2 loads} & \text{(Case II).} \end{cases} \tag{3.15}$$

To every value of the dimensionless time τ^* corresponds a critical size of the initial perturbation angle θ^* that marks the transition from a total plastic loading to a partial unloading in the structure's initial response. The results for the critical perturbation angle θ^*/T as a function of τ^* are depicted by the upper curve (force control) in Fig. 4. The conditions for a displacement control are also presented for the sake of completeness. The critical value of θ^*/T is an increasing function of time τ^* and tends to a plateau for larger values of τ^*. From the knowledge of the time and of θ^*/T one deduces from Fig. 4 which set of governing equations should be considered. Both are now discussed.

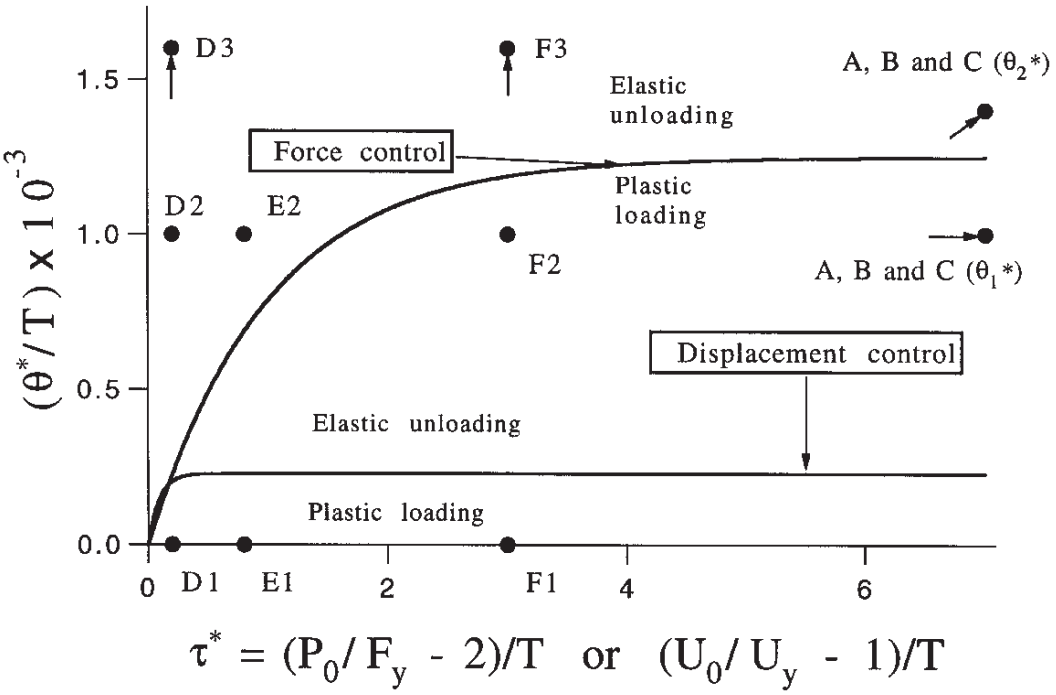

Fig. 4. The dependence of the initial loading and unloading conditions on the perturbation size θ^* and on the time at which the perturbation is applied—given here either in terms of the applied force P_0 or applied displacement U_0. The top and bottom curves correspond to the principal trajectory under a fixed force rate and a constant displacement rate, respectively.

In Case I, both supports load at the onset of perturbation and continue loading beyond that time. By adding and subtracting the internal variable rate $\dot{u}_1^{\mathrm{p}}$ and $\dot{u}_2^{\mathrm{p}}$ in (2.5) we obtain

$$\frac{\mathrm{d}P_0}{\mathrm{d}\tau}+P_0\left[1+\frac{E}{F_{\mathrm{Y}}h}\right]=2E\left[\frac{\mathrm{d}v}{\mathrm{d}\tau}+v+\frac{1}{h}\right], \tag{3.16}$$

and

$$\frac{\mathrm{d}}{\mathrm{d}\tau}\left[P_0\theta-k\theta^3\right]+\left[P_0\theta-k\theta^3+\frac{\tilde{m}}{L}\right]\left[1+\frac{E}{F_{\mathrm{Y}}h}\right]=\frac{2El^2}{L}\left[\frac{\mathrm{d}\theta}{\mathrm{d}\tau}+\theta\right], \tag{3.17}$$

respectively, with the initial conditions

$$u_a^{\mathrm{p}^*}=v_0^*-\frac{P_0^*}{2E}. \tag{3.18}$$

The solution to this problem is valid as long as the following loading conditions are maintained

$$P_0\left[1+\frac{F_{\mathrm{Y}}h}{E}\right]-2F_{\mathrm{Y}}\left[1+hv\right]>\pm\left\{\left[\frac{L}{l}\left(P_0\theta-k\theta^3\right)+\frac{\tilde{m}}{l}\right]\left[1+\frac{F_{\mathrm{Y}}h}{E}\right]-2F_{\mathrm{Y}}hl\theta\right\}. \tag{3.19}$$

Note that it follows from the initial perturbation relations in (3.3) that the inequality (3.19) is automatically satisfied at τ^* in Case I. The above nonlinear equations (3.16) and (3.17) with constraints (3.19) and initial conditions (3.18) govern the evolution of a small initial perturbation from the principal trajectory for case 1.

The linear stability of these trajectories is now discussed. From (3.4) and the imposed initial conditions (3.18) we determine, with the help of the linearized version of the nonlinear perturbation equations (3.16) and (3.17), the first time derivative of θ

$$\left(\frac{\mathrm{d}\theta}{\mathrm{d}\tau}\right)^*=\frac{E\theta^*}{F_{\mathrm{Y}}h}\frac{1+\psi}{1-P_0^*/P_{\mathrm{E}}},\quad\text{with}\quad\psi\equiv\left(\frac{\mathrm{d}P_0}{\mathrm{d}\tau}\right)^*\frac{1}{P_{\mathrm{E}}}\frac{F_{\mathrm{Y}}h}{E}=T\frac{P_{\mathrm{Y}}}{2P_{\mathrm{E}}}\frac{F_{\mathrm{Y}}h}{E}. \tag{3.20}$$

As in the equilibrium case, that first derivative is always positive for load below the Euler load. The only difference is that this rate is now an increasing function of the dimensionless number T. To discuss stability, it is thus necessary to estimate if this positive growth could be maintained beyond the onset. The only means at our disposal to check this trend is the second derivative of θ at τ^*, as it was done before for T equal zero. For that purpose, equation (3.20) is combined with the linearized version of the governing equations (3.16) and (3.17) and the force relation in (3.10) providing

$$\left(\frac{\mathrm{d}^2\theta}{\mathrm{d}\tau^2}\right)^* = \frac{E\theta^*}{F_Y h}\frac{P_0^* - P_T^*}{P_T[1-P_0^*/P_E]^2}, \tag{3.21}$$

with

$$P_T^* \equiv P_T\left(1 - T\frac{3}{2}\frac{P_Y}{P_E} - T^2\frac{1}{2}\left(\frac{P_Y}{P_E}\right)^2\frac{P_T}{P_E - P_T}\right),$$

where the T-dependent critical load P_T^* is named the '*rate-dependent tangent modulus load*' for reasons which are explained below. Note from (3.21) that the sign of the second derivative changes as the load at perturbation reaches the value of P_T^*. This change in sign marks the stability transition according to our criterion. The name of rate-dependent tangent modulus load stems from the fact that in the limit of vanishing T, P_T^* tends to the classical tangent modulus load. The surprising result is the decreasing dependence of that critical load on T according to $(3.21)_2$ which is depicted by a dashed curve in Fig. 5. This result appears to be counter-intuitive since we expect rate

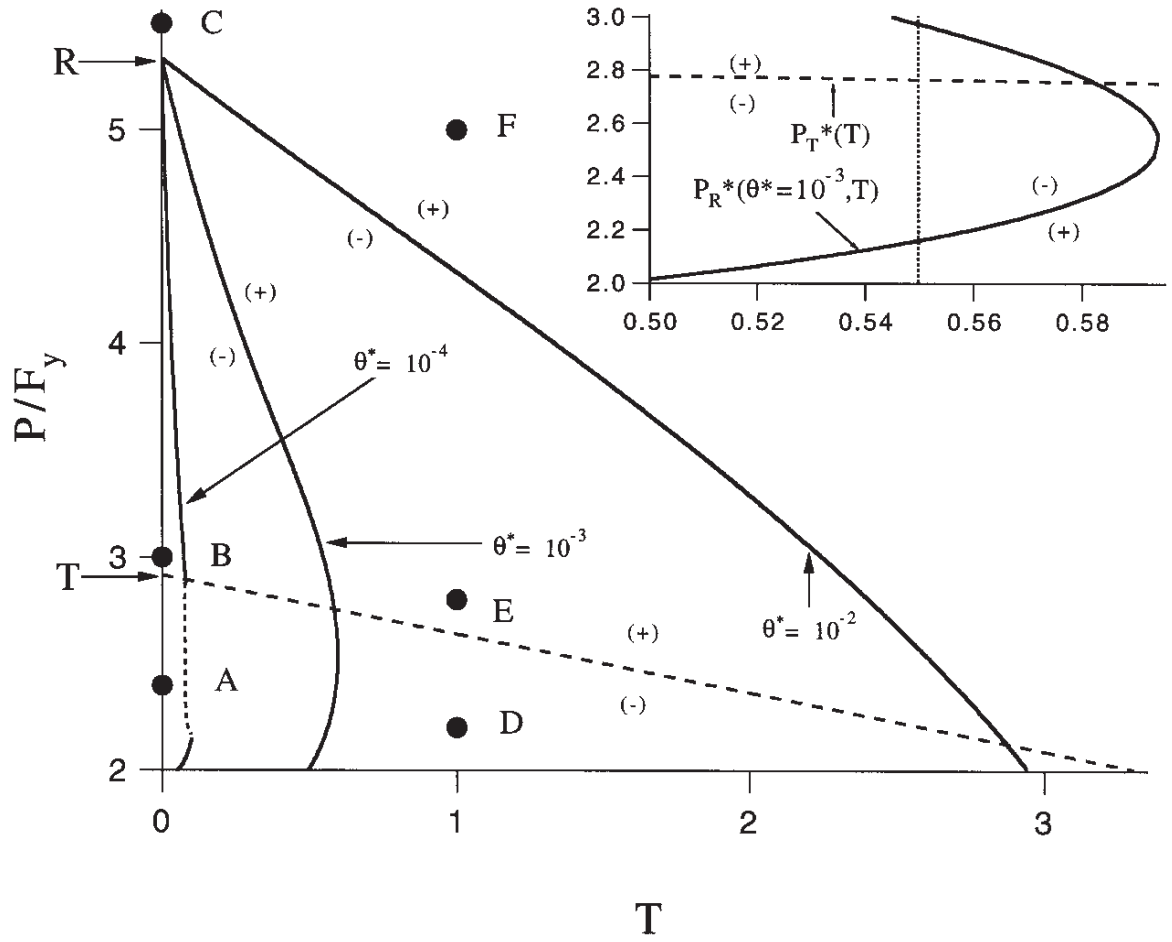

Fig. 5. Linear stability diagrams of the principal trajectory for the discrete support model under force control. If initial elastic unloading occurs, the stability threshold is the rate-dependent reduced modulus load (solid curve) which depends on the perturbation size θ^* as well as on the dimensionless number T. Note that this critical load is not always defined (dotted curve). In the absence of initial elastic unloading, the critical load is the rate-dependent tangent modulus load (dashed curve) which depends solely on T.

effects to introduce a latency for the development of any instability. This apparent discrepancy will be subsequently explained by numerical means.

The linear stability results obtained so far are valid for adequately small values of the initial perturbation θ^* which ensure the plastic loading of both inelastic supports, at least for times near the onset τ^*. If the values of θ^* are large enough, unloading of inelastic support 1 at τ^* occurs. The governing equations of the perturbed system have then to be changed accordingly, leading next to the discussion of the second alternative in (3.15).

In Case II, support 1 unloads elastically while support 2 continues to load beyond the onset. The governing equations are obtained in a manner similar to the one employed above; they read

$$v - l\theta + \frac{1}{2E}\left[-P_0 + \frac{L}{l}\left(P_0\theta - k\theta^3\right) - \frac{\tilde{m}}{l}\right] = v_0^* - \frac{P_0^*}{2E}, \tag{3.22}$$

and

$$\frac{\mathrm{d}}{\mathrm{d}\tau}\left[P_0\theta - k\theta^3\right] + \left[P_0\theta - k\theta^3 + \frac{\tilde{m}}{L}\right]\left[1 + \frac{E}{2F_Y h}\right] + \left[\frac{P_0 - P_0^*}{2F_Y h} + \left(\frac{\mathrm{d}u_1^p}{\mathrm{d}\tau}\right)_0^*\right]\frac{El}{L} = \frac{2El^2}{L}\left[\frac{\mathrm{d}\theta}{\mathrm{d}\tau} + \theta\right], \tag{3.23}$$

and should be complemented by the initial conditions (3.18). In addition, the following unloading condition for support 1 and loading condition for support 2 must be met

$$\begin{aligned} &P_0 - \frac{L}{l}\left(P_0\theta - k\theta^3\right) - \frac{\tilde{m}}{l} < 2F_Y[1 + h(u_1^p)_0^*], \\ &P_0\left[1 + \frac{F_Y h}{E}\right] - 2F_Y[1 + hv] > -\left[\frac{L}{l}\left(P_0\theta - k\theta^3\right) + \frac{\tilde{m}}{l}\right]\left[1 + \frac{F_Y h}{E}\right] + 2F_Y hl\theta. \end{aligned} \tag{3.24}$$

Note that the loading/unloading conditions (3.24) for inelastic supports 1 and 2 are automatically satisfied at τ^* in view of $(3.15)_2$. The above nonlinear equations (3.22) and (3.23) together with the initial conditions (3.18) and the constraints (3.24) govern the evolution of a large initial perturbation from the principal trajectory for Case II.

To discuss stability, we consider the linearized version of equations (3.22) and (3.23) which provides the following expression for the rotation rate

$$\left(\frac{\mathrm{d}\theta}{\mathrm{d}\tau}\right)^* = \frac{E\theta^*}{2F_Y h}\frac{1 + 2\psi + r}{1 - P_0^*/P_E}, \quad \text{with} \quad r = \frac{F_Y h}{El\theta^*}\left(\frac{\mathrm{d}u_1^p}{\mathrm{d}\tau}\right)_0^*, \tag{3.25}$$

where ψ is defined in (3.20) and r a positive scalar less than 1 in view of $(3.15)_2$. The rotation rate is always positive for the range of loading of interest and the second derivative of the angular perturbation with respect to θ at τ^* is again needed to discuss

stability. Following a procedure similar to the one employed above, that second derivative is found to be:

$$\left(\frac{\mathrm{d}^2\theta}{\mathrm{d}\tau^2}\right)^* = \frac{E\theta^*}{2F_Y h}\,\frac{1+r-qP_R/P_E}{(1-P_0^*/P_E)^2}\,\frac{P_0^*-\mathscr{P}_R^*}{P_R},$$

$$\text{with} \quad q = (\mathrm{d}P_0/\mathrm{d}\tau)^*/2El\theta^*,$$

$$\text{and} \quad \mathscr{P}_R^* \equiv P_R\,\frac{1+r-q-(E/F_Y h)\psi(3+4\psi+2r)}{1+r-qP_R/P_E}. \tag{3.26}$$

The second derivative is expressed as the product of three fractions in the right-hand-side of $(3.26)_1$. The first fraction is positive for all admissible perturbations. The sign of the second fraction is determined by its numerator which is found to be always positive since it is a slightly stronger condition that $(3.15)_2$ which defines the present Case II. The sign of the second derivative of the angular position is thus governed by the numerator of the third fraction. The change in sign occurs as the load at perturbation exceeds the value of $\mathscr{P}_R^*$ which is a function of τ^*. Consequently, the stability of the structure changes when the applied load $P_0(\tau^*)$ takes the same value as the function $\mathscr{P}_R^*(\tau^*)$ which is denoted by P_R^* and called '*the rate-dependent reduced modulus load*'. This name is explained by the fact that the critical load collapses to the classical reduced modulus load in the limit of vanishing T. With the same stability criterion introduced for Case I, we thus conclude from (3.26) that for load levels smaller than P_R^* and for adequately large perturbation θ^* (which satisfies conditions for Case II as well a the inequality $1+r-qP_R/P_E > 0$), the principal trajectory is initially stable, since the second derivative of the rotation angle is negative. For loads larger than P_R^* and for the same perturbations θ^*, the principal trajectory is initially unstable, since the second derivative in (3.26) is then positive.

Some comments are now in order concerning this new critical load called the rate-dependent reduced modulus load. Notice that unlike P_T^*, P_R^* depends not only on T but also on the size of the initial perturbation θ^*. This dependence is illustrated in Fig. 5 for the three different values of θ^* of 10^{-4}, 10^{-3}, and 10^{-2}. For the largest perturbation size, the critical load is found to be a monotonic decreasing function of T. The slope of P_R^* becomes steeper with decreasing perturbation size. However, for the two smallest perturbation sizes in Fig. 5, the dependence of P_R^* on T is not one-to-one. Considering for example $\theta^* = 10^{-3}$, we observe that P_R^* decreases as T increases until a value of, approximately, 0.62 is reached. No values of P_R^* are found for T larger than this 0.62. Furthermore, it should be noted that P_R^* is a multi-valued function of T in the interval $[0.50, 0.62]$. This dependence of P_R^* on T is even more complex for small values of the perturbation which, however, are large enough to produce initial unloading. Indeed, it is seen for $\theta^* = 10^{-4}$ that the existence of $P_R^*(\theta^*, T)$ is not always guaranteed for all values of P/F_Y, as shown by the dotted line in the interval approximately of $2.2 < P/F_Y < 2.8$.

Figure 5 is used to summarize the linear stability results for the principal trajectory. For a given number T and perturbations θ^* that satisfy the total plastic loading

conditions at τ^* (i.e. for perturbations which lie below the top $\theta^* - \tau^*$ curve in Fig. 4), the stability of the structure is governed by the P_T^* curve in Fig. 5. If the load P_0 at the onset is such that the point $(P/F_Y, T)$ lies in the region marked by a minus sign below that curve, then the column is stable. If the same point lies in the region marked by the plus sign, then an instability is predicted. For partial elastic unloading at the onset (i.e. for perturbations which lie above the top $\theta^* - \tau^*$ curve in Fig. 4), the stability of the structure is controlled by the curve $P_R^*(\theta^*, T)$ in Fig. 5. Some paradoxical results could then be obtained due to the shape of these curves as it is now commented for the special example of T equal to 0.55 which is within the interval for which $P_R^*(\theta^*, T)$ is multivated (see dotted line in insert of Fig. 5). In that instance, if the angular perturbation is very small, both supports load at the onset and stability, governed by $P_T^*(T)$, is warranted unless the load is larger than $2.77F_Y$, a value which is smaller than P_T. If the perturbation is sufficiently large to induce unloading at the onset then the stability verdict is different. Indeed, a perturbation size of 10^{-3} is sufficient to destabilize the system for a load as small as the yield load and smaller than approximately $2.2F_Y$, insert of Fig. 5. The same perturbation leads to a stability verdict for loads in the interval $[2.2F_Y, 2.97F_Y]$ and to a conclusion of instability above that interval. This rather peculiar response will indeed be confirmed during the nonlinear analysis which is presented next.

3.1.3. *Nonlinear stability analysis of the principal trajectories* ($T \neq 0$)

The results of the numerical solution of the perturbation problem under force control are shown in Fig. 6 in which the evolution of the rotation rate $\theta_{,\tau}$, normalized by its initial value $|\theta_{,\tau}^*|$, is presented as a function of the dimensionless force P/F_Y. A quasi-static loading with $T = 10^{-4}$ is considered in Fig. 6(a), while Fig. 6(b) corresponds to a more rapid loading with $T = 1$. All model parameters are identical to those used for the stability of the principal equilibrium calculations in Fig. 3.

For the quasi-static loading rate, the results in Fig. 6(a) are calculated for two perturbation sizes $\theta_1^* = 10^{-7}$ (solid line) and $\theta_2^* = 10^{-4}$ (dotted line). The results of three simulations are presented corresponding to three different onset times and thus to three different levels of force. The curves starting at point A are for a load less than P_T while those initiating from B and C are obtained for perturbation load comprised between P_T and P_R and larger than P_R, respectively. In view of the slow loading rate, the numerical values of P_T^* and P_R^* differ imperceptibly from their time-independent counterparts P_T and P_R as seen from Fig. 5. The numerical values of the perturbation θ^* are chosen so that the smallest one (θ_1^*) corresponds to loading of both supports at the onset and the largest of the two (θ_2^*) corresponds to unloading of one support at the onset, as can be verified in Fig. 4 by checking the position of points A, B and C. The small arrows on Fig. 4 pointing to those particular points mark the fact that they are outside the range of the plot. They nevertheless are presented to visualize their position with respect to the relevant curve.

Looking at point A in Fig. 6(a), we observe that for both perturbation sizes the rotation rate curves have identical negative initial slopes, in agreement with the linear stability criterion which predicts that the critical load P_T^* is independent of the imperfection size. At point B, the slope is positive for the small perturbation size and

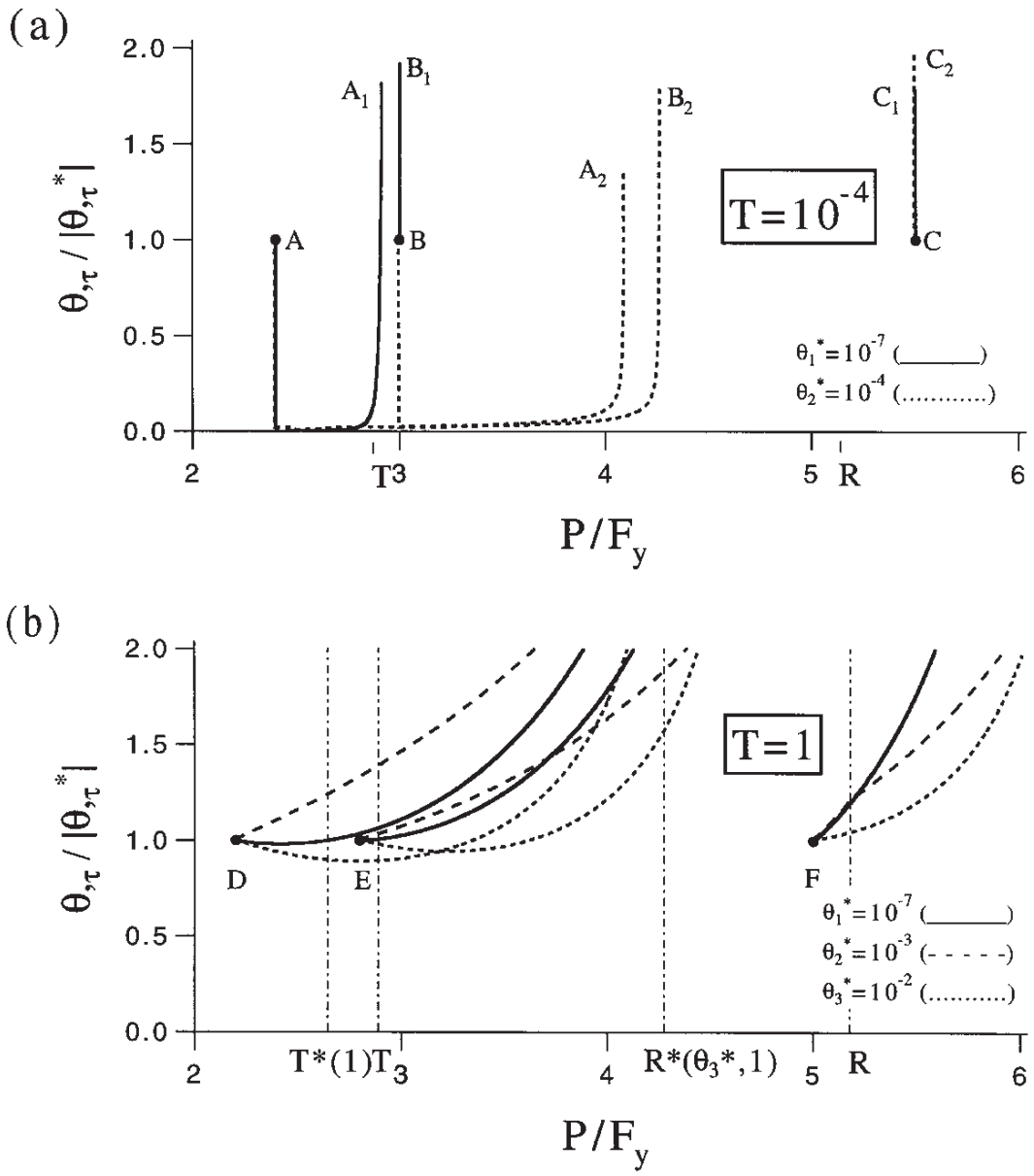

Fig. 6. The evolution with time of a small perturbation from the principal trajectory for the rate-dependent discrete model under force control. The numerical calculations for a quasi-static loading rate ($T = 10^{-4}$) are depicted in (a) and for a rapid loading rate ($T = 1$) in (b). Several perturbation sizes were applied at three different force levels. The initial slopes confirm the linear stability predictions found with the help of Figs 4 and 5.

negative for the larger size. This result is also in agreement with our criterion as can be judged from the position of point B in Fig. 5. It is seen that this point B is above P_T, signalling an instability if both supports load at the onset, and below P_R corresponding to a stable prediction if the perturbation induces partial unloading. Observe now from Fig. 6 that the slopes are positive at point C for both perturbation sizes. This is also in agreement with the linear stability predictions, since point C in Fig. 5 lies above both the tangent and the reduced modulus loads. The long term nonlinear evolution depicted in Fig. 6 is of course not predicted by our linear analysis and is due to the existence of a maximum load in the equilibrium solutions (see

Fig. 2(b)). Indeed, all the curves in Fig. 6(a) eventually increase without bound at some finite value of P/F_Y. Notice the peculiar feature of the two cases starting at A for which the latency period prior to the final development of the instability is smaller for the smallest of the two perturbations. This counter-intuitive result can be explained by the stabilizing influence of the partial elastic unloading at the onset which is not present for the smaller size perturbation.

The stability results of the same structure subjected to a more rapid loading rate ($T = 1$) are presented in Fig. 6(b) for three different initial perturbation sizes of 10^{-7}, 10^{-3} and 10^{-2} corresponding to solid, dashed and dotted curves, respectively. The simulations reported have been conducted for three different levels of force. Point D corresponds to a load below $P_T^*(1)$ while points E and F are in the two intervals $[P_T^*(1), P_R^*(10^{-2}, 1)]$ and $[P_R^*(10^{-2}, 1), P_R]$, respectively, as can be seen in Fig. 5. Note that P_T^* is only a function of T and that the two arguments of P_R^* introduced above are, first, θ^* and, second, T. The same order is used throughout the rest of the paper.

Looking at the curves originating from point D in Fig. 6(b), we observe that the slope is initially positive (instability) for the intermediate perturbation size and negative otherwise (stability). To compare these results with our linear stability predictions, note that the smaller perturbation size leads to plastic loading while the two largest sizes result in partial unloading (points D1, D2 and D3 in Fig. 4). Considering now the position of point D in Fig. 5 with respect to $P_T^*(1)$, $P_R^*(10^{-3}, 1)$ and $P_R^*(10^{-2}, 1)$ we predict stability for the smallest and largest perturbation size and instability for the intermediate size. Those predictions are thus in agreement with the nonlinear evolution at the onset. The analysis of point E in Fig. 6(b) is similar and left to the reader.

One of the interesting new results in Fig. 6(b) is that the instability is observed for the smallest perturbation size even thought the perturbation force is lower than the tangent modulus load (points D and E). This nonlinear evolution is well predicted by our stability criterion and confirms the possibility to destabilize a structure above the rate-dependent tangent modulus load which, again, is smaller than P_T. Similarly, the curves originating form point F in Fig. 6(b) have all an initial positive slope signalling instability for any perturbation size. The first and second perturbations lead to continuous loading at the onset (points F1 and F2 in Fig. 4) while the largest size (point F3) still induces partial unloading. However, as can be seen from Fig. 5, point F is above both $P_R^*(10^{-2}, 1)$ and $P_T^*(1)$ and linear instability always predicted.

To complete our non-linear analysis, we discuss the long term instability development which is not necessarily captured by our linear stability criterion. All the curves in Fig. 6(b) increase eventually monotonically with the applied load. In contrast to Fig. 6(a), they lack a sharply defined bend. Note that this long-term development is not in contradiction with the linear stability predictions for T equal 1 which stipulates that a judicious choice of a perturbation size can destabilize the structure at any force level.

3.1.4. *Sensitivity to imperfections*

So far we have studied the stability of the principal equilibria and the principal trajectories of the perfect strain-rate dependent model. The presence of initial imper-

fections is unavoidable in any experimental realization of the model structure. We must therefore, investigate the link between the imperfection sensitivity analysis (often proposed in the literature as the only means to assess stability) and our linear stability predictions of the principal trajectories. To be consistent with the stability calculations presented so far, the initial imperfection of the structure is modeled by a constant perturbation moment $\tilde{m}$ applied at the beginning of the loading process ($P_0 = 0$). From the perturbation relations in (3.3), we find the equivalent initial imperfection angle $\theta^* = \tilde{m}/LP_E$. The governing equations for the structure are still given by (2.1)–(2.6). These equations are solved numerically under force control for different values of the dimensionless characteristic time T and different sizes of initial imperfection θ^*. The model parameters used in these investigations are identical to those employed for the stability calculations of the principal trajectories.

The simulations reported in Figs 7(a–b) and (c–d) are for a quasi-static loading rate ($T = 10^{-4}$) and for a more rapid loading rate ($T = 1$), respectively. For each value of T, three values of the imperfection size θ^* are considered. The results in Fig. 7(a) depict the rotation θ as a function of the dimensionless applied force P/F_Y. As expected from the equilibrium solution for quasi-static conditions in Fig. 2(b), the smaller the initial imperfection the closer the P–θ curve is to the bifurcation solution (solid curve) emanating from the tangent modulus load P_T. Once a maximum load is reached, the rotation increases without bound, as expected for force control. Note that there is no difference here between the long term evolution of the imperfection analysis and the nonlinear stability analysis, Fig. 6(a).

Of additional interest is the initial evolution of the instability which is illustrated in Fig. 7(b) by depicting the rotation rate $\theta_{,\tau}$ in the range of 10^{-6} as a function of the normalized applied force P/F_Y. These graphs are complex due to the presence of repeated sudden changes in the rate of rotation which we shall try to explain starting with the smallest initial imperfection of $\theta^* = 10^{-7}$ (results in dotted curve). The spike near but prior to the elastic limit $P_Y = 2F_Y$ of the perfect column is due to the yield of support 2 which is marked by a solid triangle, Fig. 7(b). The same symbol is used on that figure for every change in loading conditions. The column is more compliant and the rotation rate increases until the second support yields (tip of spike). The rotation rate then surprisingly decreases to remain close to zero until the applied load becomes close to the tangent modulus load. Then, the rotation rate increases with a discontinuity in slope due to the unloading of a support. To help the reader, the various portions of those curves are marked by the symbols (E/E), (E/P) and (P/P) referring to an elastic response of the two supports, of only one support and to the plastic response of the two supports, respectively.

Compare now this curve for $\theta^* = 10^{-7}$ with the nonlinear stability results, curve (A–A_1) in Fig. 6(a), obtained for the same imperfection size to understand this complex response. The shapes of these two curves are identical in that instance establishing the similarity between nonlinear stability analysis and imperfection analysis. Results for this quasi-static process are also in line with our linear stability predictions since the instability initiates close to the tangent modulus load.

A similar interpretation can now be provided for the intermediate imperfection size of 5×10^{-5}, plotted with a dashed–dotted curve in Fig. 7(b). Note again that the first

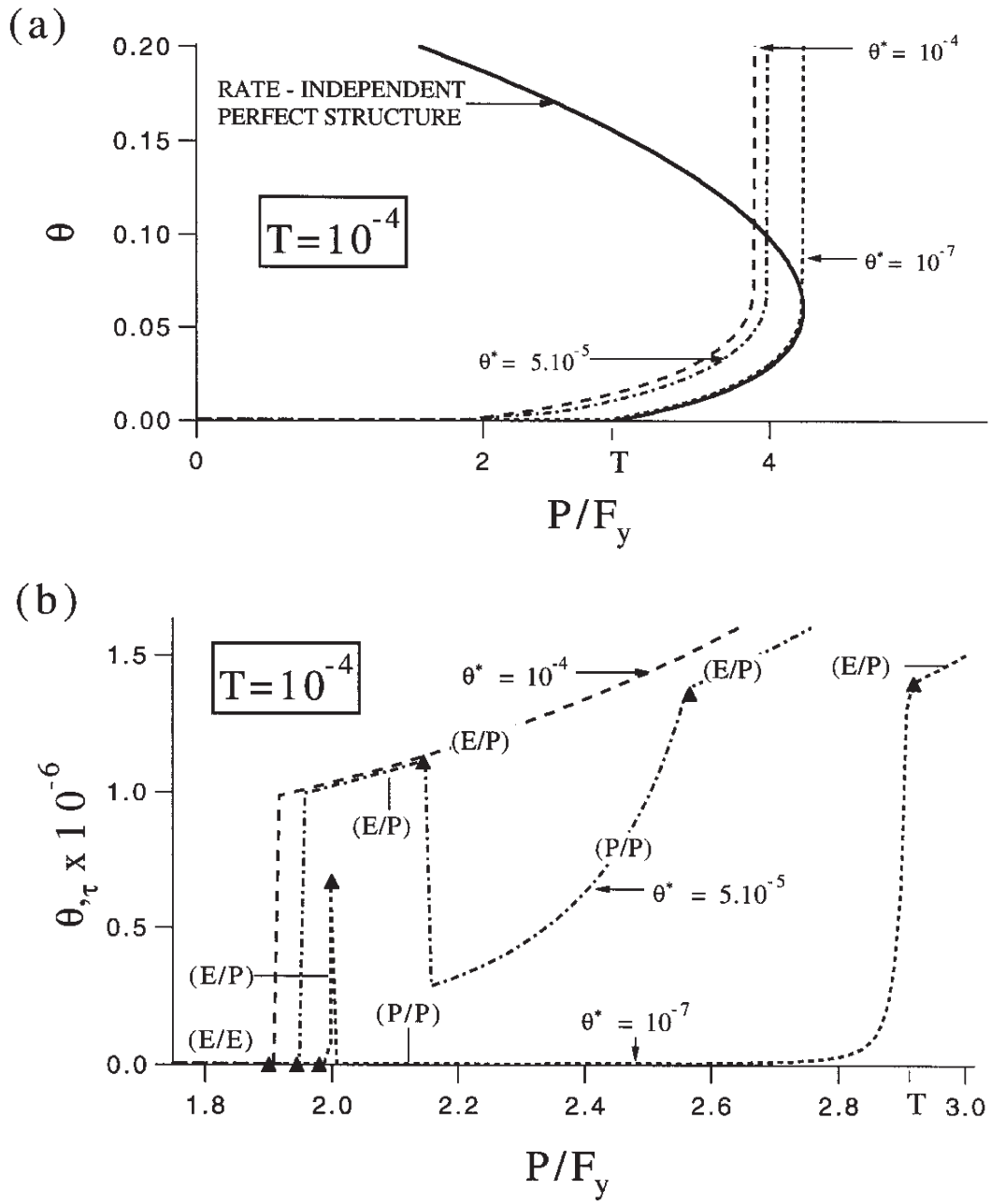

Fig. 7. The results of the imperfection sensitivity analysis of the rate-dependent discrete model under force control are shown here in terms of the evolution with time of the angular position (a, c) and its rate of change (b, d). The graphs (a) and (b) correspond to a quasi-static loading rate ($T = 10^{-4}$) and (c) and (d) to a rapid loading rate ($T = 1$).

yield of support 2 leads to an increase of the rotation rate. At a difference with the smallest imperfection discussed above, the rotation rate starts to increase significantly prior to the tangent modulus load. A similar behavior is observed for the largest imperfection size and is characterized by the absence of any permanent displacement on support 1. Such a response is of course not detected by our linear stability for the following reason. The linear stability analysis is valid for the fundamental solution and thus can only be extended to imperfection analysis if the relative difference in internal variables of the two supports remains small compared to one. The validity

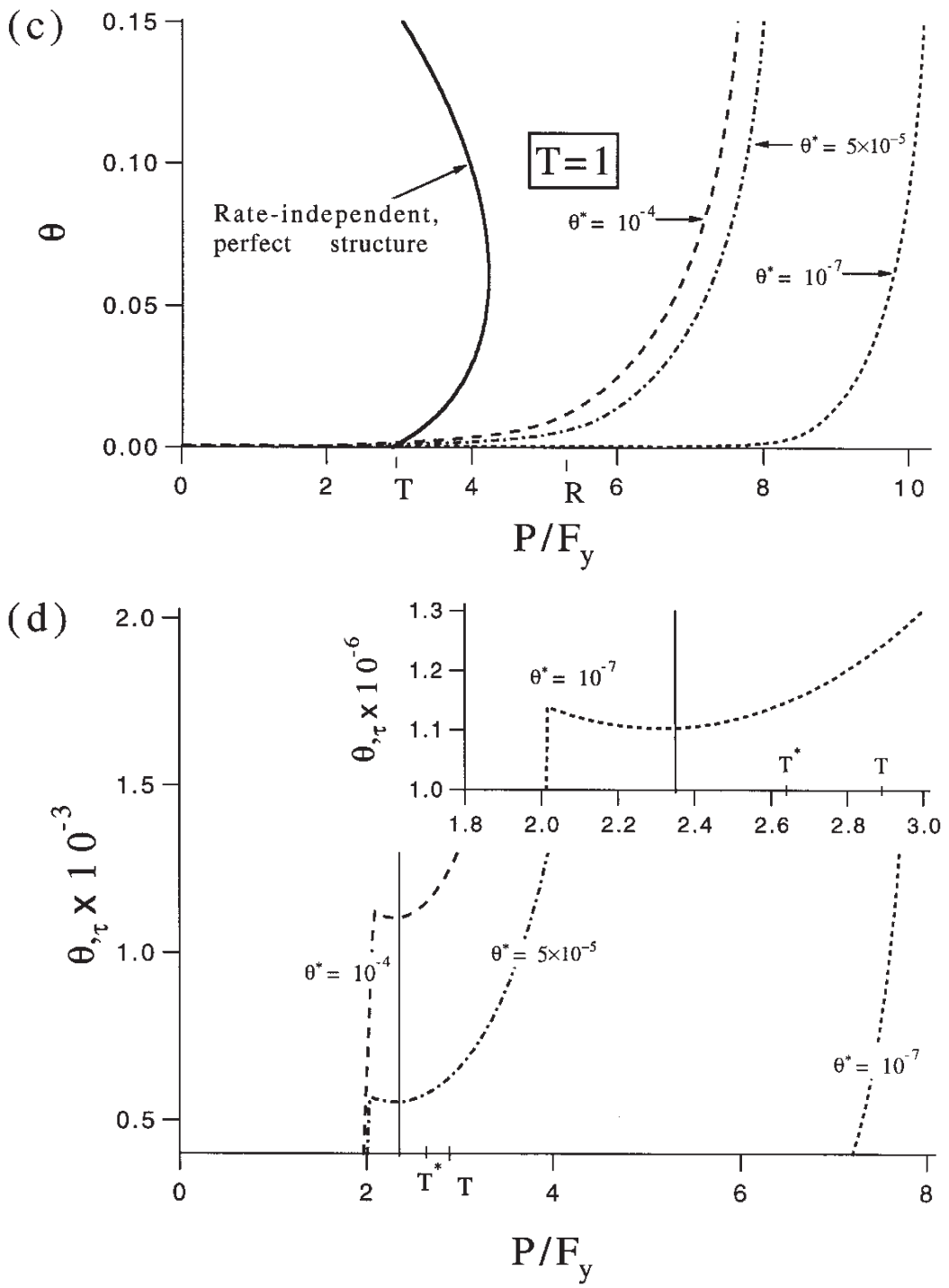

Fig 7 (*continued*)

of this assumption for our imperfection analysis can be evaluated from plots (a), (b) and (c) of Fig. 8 which depict the evolution with the applied loading of the support internal variables. In Fig. 8(a), corresponding to the smallest imperfection, the two internal variables are basically identical until the tangent modulus load is reached and our linear stability predictions apply. However, in Figs 8(b) and (c), it is clear that the hypothesis of equal permanent displacement is violated and our criterion cannot be of any help.

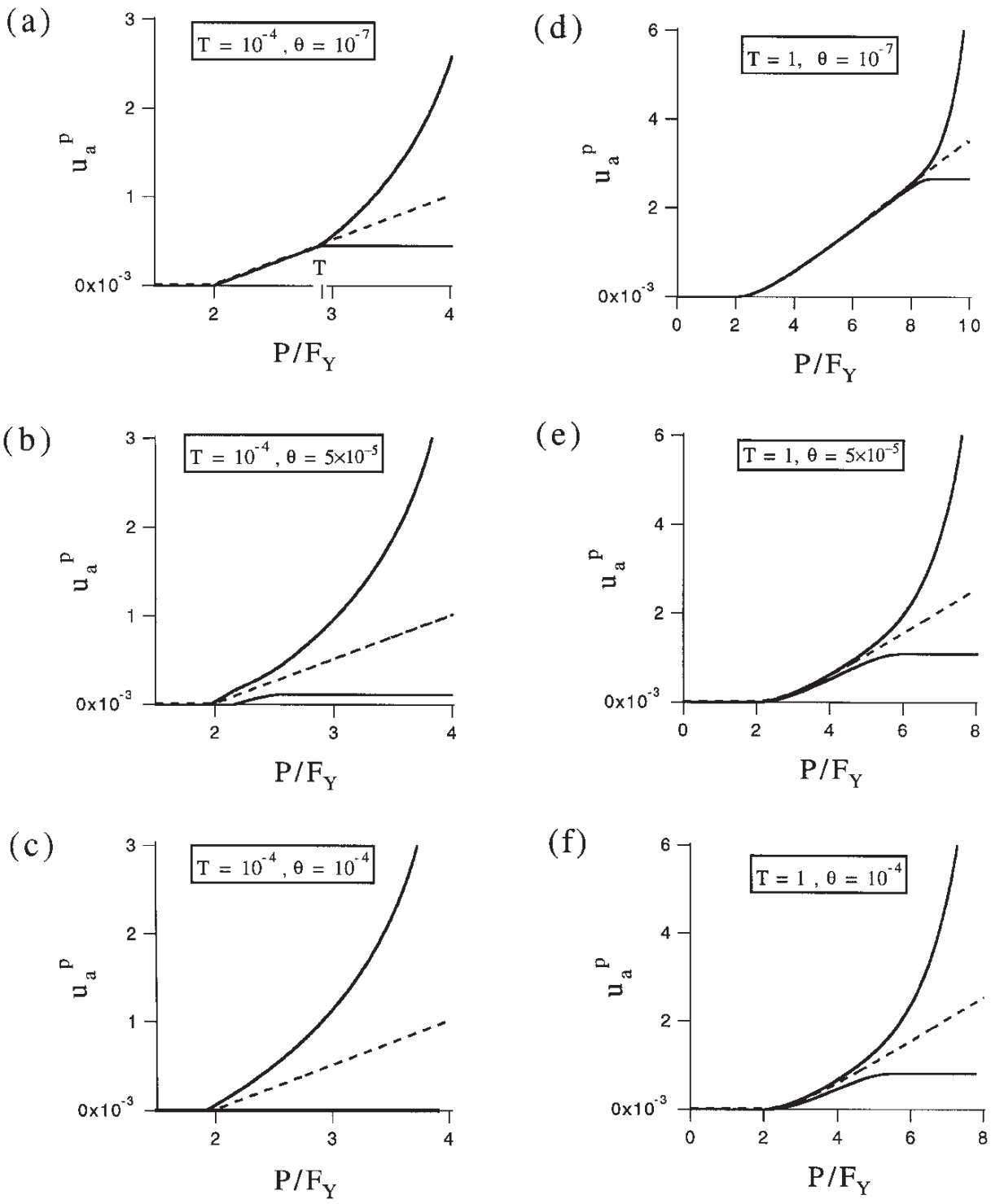

Fig. 8. The accumulated permanent displacement (internal variables) of the two supports during the imperfection analysis presented in Fig. 7 for the two values of T and the three sizes of imperfection. It is only if these two internal variables remain close to their fundamental solution counterpart at the same applied load that the linear stability predictions describe accurately the imperfection development.

We now continue the analysis of the imperfection sensitivity study for T equal to 1. The evolution of the angular position and of its rate of change with time are presented in Figs 7(c) and (d) and the corresponding evolution of the internal variables

in Figs 8(d–f). The first observation from Fig. 7(c) is the considerable delay in the development of the rotation of the column compared to the quasi-static case. This long-term development of the instability is in line with what is known concerning rate effects in various instability problems: viscosity results in a latency period prior to the instability development. A consequence of this delay is that the solutions with imperfections are very close to the fundamental solution, justifying our stability analysis for loads much larger than the classical tangent and reduced modulus loads. Since our criterion is applicable to the initial stage of the instability development, let us now focus on the initial evolution of that instability, depicted in Fig. 7(d). For the three imperfection sizes, the two supports yield close to the first yield of the perfect column. The rotation rate rises sharply then decreases until a normalized load of 2.32 (marked by a vertical line) is reached which marks the onset of rapid growth. Note that the decrease after yield was anticipated by the linear stability predictions. Furthermore, increase in rotation rate occurs before the classical P_T is reached. More precisely, this imperfection analysis indicates that the influence of T in decreasing the critical load is even more important than predicted with our linear stability criterion since the instability initiates prior to the reach of $P_T^*(1)$, Fig. 7(d). This agreement between linear stability predictions and imperfection sensitivity studies is justified by the small difference between the two internal variables of the models around the critical load, Figs 8(d–f).

In conclusion, our linear stability criterion does provide the correct information on the initial development of an imperfection if the internal variables of the model remain close to the values taken along the fundamental solution. It should be mentioned that if this hypothesis is not respected, one's only alternative is to develop a similar criterion based on the actual trajectories and not on the fundamental solution, as suggested and explored by Tvergaard (1985).

4. Stability of a Shanley column with continuous support

The dependence of the rate-dependent reduced modulus load on the perturbation size can be better appreciated with the introduction of continuously distributed support, as considered in our second model, since the extent of the unloading zone is then accurately determined. In this section, we first consider the stability of principal equilibria ($T = 0$) and then of principal trajectories ($T \neq 0$). Results for both force and displacement boundary conditions are presented. Before proceeding, the initial conditions for the stability analysis are discussed.

It has been shown in Section 3.1 that the perturbations in internal variables can be disregarded compared to the perturbation in elastic displacement. Combining this information with the equilibrium equations (2.14), the kinematics relation (2.15) and the continuum version of the constitutive equations (2.4)–(2.6), we obtain the initial perturbation relations which are independent of the type of boundary conditions and are analogous to (3.3). Note that the Euler load P_E of the second model is still given by (2.19) and that perturbations for the elastic displacements in (3.3) should be modified to read: $\tilde{u}^e(x) = x\theta^*$. This information is used for the derivation of the size

of the unloading zone at the onset. To this end, observe that the coordinate of the unloading zone $\bar{x}$ is defined by the requirement that the internal variable rate vanishes at this point: $\dot{u}^{\mathrm{p}}(\bar{x}) = 0$. The viscosity law (2.5) provides the necessary relation to determine $\bar{x}$

$$F(\bar{x}^*) = F_{\mathrm{Y}} l[1 + h u^{\mathrm{p}}(\bar{x}^*)], \tag{4.1}$$

at the onset.

4.1. *Stability of principal equilibrium states* (T = 0)

Linear and nonlinear results are now presented for the case of principal equilibria. For sake of conciseness, only new result are presented and the algebra is limited to a minimum. The calculation of the initial extent of the unloading zone is the first step of the linear stability analysis of equilibria. The condition in (4.1) combined with the initial perturbation conditions (3.3) permits to conclude that

$$\bar{x}^* = 0, \tag{4.2}$$

for any load level and for both types of boundary conditions. Note that a similar independence of the extent of the unloading zone from the applied load and boundary conditions was also found by numerical means for continua (Massin, 1994). This result differs from the unloading zone size found for the bifurcation analysis and its consequence for the stability thresholds will become apparent in what follows.

The calculations of the linear stability threshold for the second model follows the same steps as for the first model. The rotation rate at the onset is given by (3.8) and is always positive until the Euler load is reached. This result holds for both force and displacement control. Consequently, since no information can be extracted from this first derivative, we turn again our attention to the second time-derivative of the angular position which, for force control, is found to be

$$\left(\frac{\mathrm{d}^2\theta}{\mathrm{d}\tau^2}\right)^* = \frac{E\theta^*}{2F_{\mathrm{Y}}h}\left[1 + \frac{E}{8F_{\mathrm{Y}}h}\right]\frac{P_0/P_{\mathrm{Rc}} - 1}{(P_0/P_{\mathrm{E}} - 1)^2}, \quad \text{with} \quad P_{\mathrm{Rc}} \equiv P_{\mathrm{E}}\frac{1 + E/8F_{\mathrm{Y}}h}{1 + 5E/8F_{\mathrm{Y}}h}. \tag{4.3}$$

The change in sign of the second derivative defines the stability threshold at P_{Rc} which is the rate-dependent reduced modulus load for T equal zero. The letter c in subscript is reserved to quantities determined for the continuous support model and which differ from their counterpart obtained for the first model. The critical load P_{Rc} is larger than its rate-independent counterpart P_{R} given in (2.19). This conclusion can be checked from Fig. 9 which shows the critical loads P_{R}, $P_{\mathrm{R}'}$ and P_{Rc} as a function to the dimensionless number $E/(F_{\mathrm{Y}}h)$. This critical load P_{Rc} is bounded from above and below by the reduced modulus loads found for displacement and force control, respectively. Note that these three loads tend to the Euler load as the plastic hardening modulus h tends to infinity and that the difference between P_{R} and P_{Rc} is maximum in the limit of perfect plasticity.

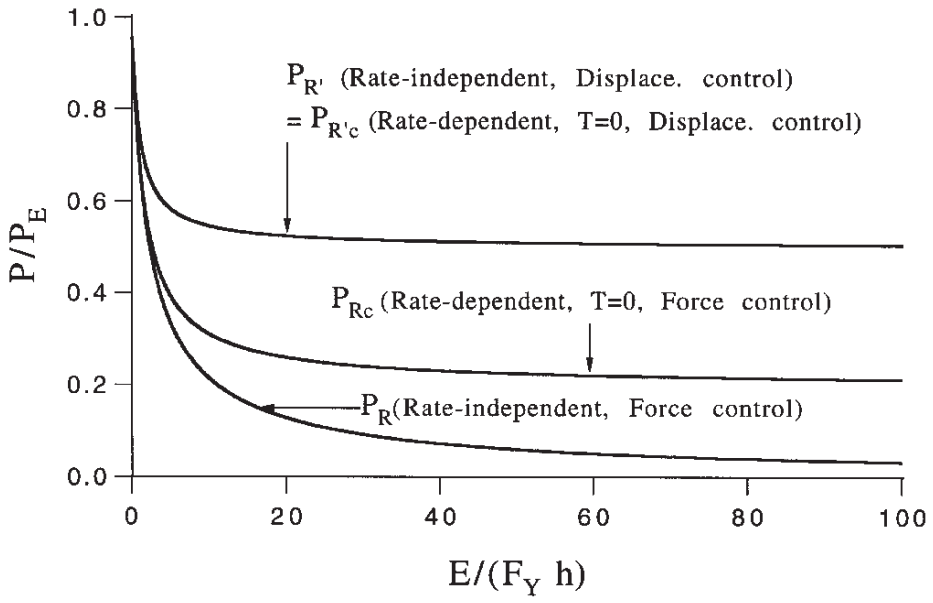

Fig. 9. Comparison between various stability thresholds presented as function of the dimensionless number $E/F_Y h$ for the continuous support model. Two of these loads, known for the rate-independent column, are the reduced modulus load P_R and $P_{R'}$ for force and displacement control, respectively. The two others are the rate-dependent reduced modulus loads as T approaches zero, for force and displacement control. Only for the case of displacement control do the two stability thresholds coincide.

The linear stability analysis of principal equilibria with displacement control provides the same expression for the second time-derivative of the column's angular position as for the first model [see (A.2)]. Consequently, the stability threshold $P_{R'c}$ coincides with the reduced modulus load of the rate-independent structure $P_{R'}$, as it was found in the first model. This result is not surprising, since the size of the initial unloading zone at the onset is the same for the two analyses.

The new result above, which deserves nonlinear validation, concerns the stability limit under force control. The evolution in time of the rate-dependent column perturbed from an initial equilibrium position is presented in Fig. 10 for four load levels corresponding to 0.11, 0.98, 1.31 and 1.63 times P_R. These numbers are selected so that the applied force falls in between the various critical loads of interest, as indicated in Fig. 10 and discussed thereafter. The results are obtained with a fourth order Runge–Kutta scheme for the time discretization and a trapezoidal integration rule of the constitutive law along the column's basis. Perturbations applied at load levels smaller than P_R confirm our linear stability prediction. The rate of rotation decreases and a new equilibrium is reached. Note that the lateral spring is ignored in these calculations and the nonlinear results presented for the first model, which predict runaway instability slightly below P_R, cannot be duplicated here. Furthermore, we observe that between P_R and P_{Rc} the initial rotation rate first decreases as predicted by the linear theory. However, nonlinear effects are sufficiently strong to prevent the column to reach a new equilibrium state and the rotation rate increases without bound in a second stage. For load larger than P_{Rc}, the angular rate initially increases as appropriately predicted by the linear analysis.

To conclude the stability analysis of equilibria, one should stress that the rate-

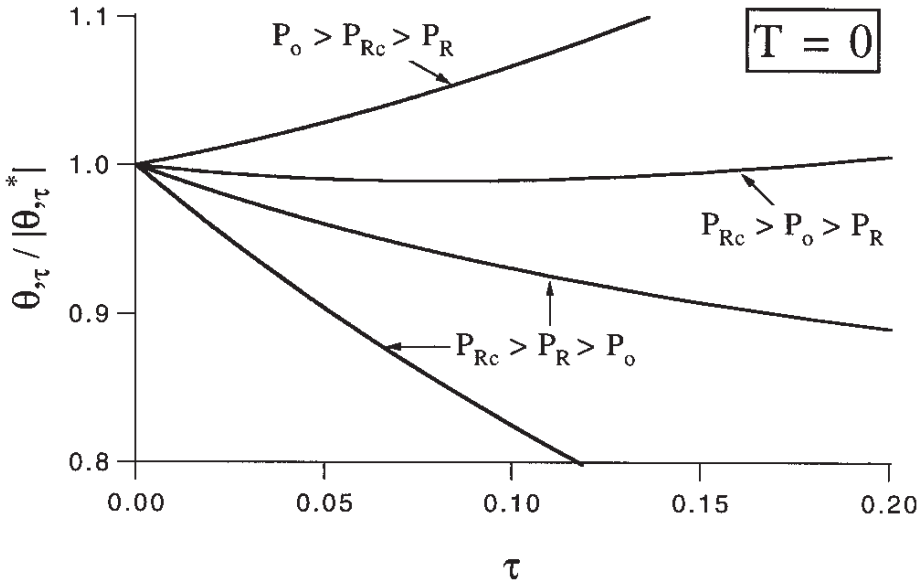

Fig. 10. Evolution with time of the normalized rotation rate for four equilibria of the continuum support model under force control. The rotation rate initially decreases if the equilibrium load is less than P_{Rc} and increases otherwise. However, the nonlinear evolution for a load smaller than P_{Rc} and larger than P_{R} confirms the classical verdict of instability.

dependent stability limit exceeds the classical reduced modulus load for force control. The two stability thresholds coincide only for displacement control. These results are explained by comparing the extent of the initial unloading zones.

4.2. *Stability of principal trajectories* (T $\neq$ 0)

The extent of the initial unloading zone for the case of perturbation from a principal trajectory is found using the same argument as above and reads

$$\bar{x}^*\theta^* = -\frac{F_{\mathrm{Y}}h}{E}\left(\frac{\mathrm{d}u^{\mathrm{p}}}{\mathrm{d}\tau}\right)_0^*, \tag{4.4}$$

with the obvious constraint that $-l < \bar{x}^* < l$. The lower bound combined with (4.4) provides the following condition for the presence of elastic unloading

$$\frac{F_{\mathrm{Y}}h}{El}\left(\frac{\mathrm{d}u_0^{\mathrm{p}}}{\mathrm{d}\tau}\right)_0^* - \theta^* \begin{cases} > 0 \Rightarrow \text{no unloading occurs} \\ < 0 \Rightarrow \text{unloading does occur} \end{cases}. \tag{4.5}$$

The expressions for the internal variable $u_0^{\mathrm{p}}(\tau)$ depend on the type of boundary condition. It is a matter of algebra to verify that the derivatives of the internal variable along the principal branch are similar to those found in the first model. Note, however, that at a difference with the rate-independent case, there is a limit to the size of the initial unloading zone: it is found to be restricted to the right-hand-side of the column ($\bar{x}^* \leqslant 0$).

We now discuss the stability threshold along the principal trajectories. The calculations, although more involved, are analogous to the ones presented for the discrete

case and will not be recorded. The rate-dependent tangent modulus load P_{T}^{*} of the second model is identical to the one obtained for the first model (3.21). It is thus a decreasing function of T tending towards the classical tangent modulus load for vanishing values of T. This critical load P_{T}^{*} is obtained for perturbation that obeys the first condition in (4.5). If the second condition applies it is then the rate-dependent reduced modulus P_{Rc}^{*} which is obtained. The discussion of that critical load is now restricted to the case of force control and to the limit taken for vanishing T. That limit is found to be precisely the critical load P_{Rc} obtained for a zero value of T for the following reason. According to (4.4), the limit taken by the extent of the plastic zone $\bar{x}^{*}$ is zero since the perturbation size is fixed and the rate $\mathrm{d}u_0^{\mathrm{p}}/\mathrm{d}\tau$ tends to zero with T. It is thus of no surprise that the limit taken by P_{Rc}^{*} is P_{Rc} since the two are then associated with the same extent of the unlaoding zone.

This argument is taken one step further to conclude this section. For the limit taken by P_{Rc}^{*} as T vanishes to be different from P_{Rc} it is necessary that $\bar{x}^{*}$ does not tend to zero. This is possible, according to (4.4), if the limit analysis allows the second small parameter, the perturbation size θ^{*}, to be commensurate to T. Consider for example θ^{*} to be proportional to T and obtain from (4.4) a limit for $\bar{x}^{*}$ which is negative but non-zero. The limit of P_{Rc}^{*} is then found to differ from P_{Rc}. It is thus possible with the appropriate limiting process, to select a limit to the rate-dependent reduced modulus load which differs from P_{Rc}.

5. Generalization of the linear stability criterion to solids

The generalization of the stability criterion to viscoplastic continua is now outlined. Only a brief description of the pertaining arguments is provided here, a more detailed being found in Triantafyllidis et al. (1997). We consider a strain-rate dependent solid with an instantaneous elastic response which is subjected to a known loading history in time through externally applied tractions or boundary displacements. We are concerned with the initial development of the instabilities from principal trajectories which have displacement, stress and internal variable fields function of the dimensionless time τ.

A perturbation is applied at the boundary at time τ^{*} and the solid's response is estimated by following the resulting perturbation in the displacement field $\tilde{\mathbf{u}}(T, \tau)$ for all τ greater than τ^{*}. As for the two structural models considered above, it is expected that the internal variable fields of the solid at τ^{*} are unaffected by that perturbation since it is then the instantaneous elastic response of the solid that governs the perturbation at the onset. The difficulties are the same as in the discrete model case, i.e. we are faced with the analysis of a non-autonomous system of linear differential equations, whose time-dependent coefficients have the additional difficulty of the presence of discontinuities (due to the eventual change of loading/unloading conditions). It is for this reason that we again propose a stability criterion based on the initial response of the perturbed system at τ^{*}, in which the role of the angle θ in the discrete system is now played by the norm of the perturbation $\|\tilde{\mathbf{u}}\|$. That perturbation in the displacement field is determined by the perturbation in loading applied at the

boundary which plays the role of the moment $\tilde{m}$ in this paper. We first concentrate on the stability limit in the absence of any unloading upon perturbation and postpone to future work the issue of detecting the extent of the elastic zones at the onset of perturbation. The principal solution satisfies pointwise the plastic loading condition, the perturbation problem is linearized and the norm of the initial perturbations is conveniently normalized.

The linear version of the rate-form of the principle of virtual work provides a linear operator relating perturbation in velocity $\tilde{\mathbf{u}}_{,\tau}$ and displacement $\tilde{\mathbf{u}}$. This operator is based on the instantaneous elastic response of the solid of interest and remains positive definite as long as the applied load is smaller than the Euler load. This result is similar to what is found here for the rotation rate $\theta_{,\tau}$. For that reason, it is proposed to derive a stability criterion to examine the initial evolution of $\|\tilde{\mathbf{u}}_{,\tau}\|$, the L_2 norm of the first time-derivative of an arbitrary perturbation at the onset. If the maximum initial rate of change of this norm over all admissible perturbations is negative, i.e. if all possible velocity perturbations have their norm decreasing at τ^*, then the trajectory under investigation is said to be initially stable. The mathematical form of the proposed stability criterion thus depends on the sign of a scalar Λ which is defined by

$$\Lambda \equiv \max \frac{1}{2} \left\{ \frac{\mathrm{d}}{\mathrm{d}\tau} \|\tilde{\mathbf{u}}_{,\tau}\|^2 \right\}_{\tau^*}, \quad \forall \|\tilde{\mathbf{u}}_{,\tau}\|_{\tau^*} = 1. \tag{5.1}$$

If Λ is found to be negative for all admissible perturbation at time τ^* then the trajectory is said to be stable at that time. The existence of a perturbation with a positive Λ signals an instability. The stability parameter Λ can be equivalently rewritten as

$$\Lambda = \max \left\{ \langle \tilde{\mathbf{u}}_{,\tau}, \tilde{\mathbf{u}}_{,\tau\tau} \rangle \right\}_{\tau^*}. \tag{5.2}$$

To find this parameter, it is necessary to obtain the linear operator $\mathscr{L}$ that relates the first and second derivatives with respect to time of the perturbation in displacement. This operator is formally obtained in Triantafyllidis et al. (1997) by combining the linearized version of the first and second derivative with respect to time of the principle of virtual work. The research for the maximum in (5.2) is then equivalent to the search of the dominant eigenvalue of the self-adjoint part of the operator $\mathscr{L}$. A sufficient criterion for instability is that at least one eigenvalue of $\mathscr{L}$ has a positive real part since we can then show that Λ is positive.

The above discussion pertains to arbitrary values of the dimensionless number T. As for the two structural problems discussed above, it is of interest to determine the stability threshold as T tends to zero. It is found above that the rate-dependent tangent modulus converges to the classical tangent modulus load of the rate-independent structure as T vanishes. In the continuum case, one does capture Hill's critical load for the corresponding rate-independent solid in the limit of a vanishing T, as discussed by Triantafyllidis et al. (1997).

6. Conclusion

A linear stability criterion for strain-rate sensitive, elasto-plastic solids and structures is proposed and validated with the help of two finite degree of freedom structural

models reminiscent of Shanley's column (Shanley, 1947). This criterion accounts for the presence of two time scales, the first defined by the relaxation time of the viscous material and the second by the applied loading rate. The corresponding stability results depend on the ratio T of the two characteristic times and on the size of the initial perturbation.

Linear perturbation methods have been proposed in the past to capture the initiation of instabilities in elastic–viscoplastic solids and structures. The main difficulty is that the resulting differential equations governing the perturbation evolution have time-dependent coefficients which are frequently discontinuous functions of position due to unloading. Disregarding this time-dependence results in the commonly used frozen-coefficient approximation. The stability criterion proposed, although based on an investigation of the linearized system at the onset of perturbation, accounts for the time dependence of the fundamental solution and should thus overcome the shortcomings of the frozen coefficient assumption. More specifically, for the two Shanley-type columns considered here, the criterion is based upon the change in sign in the second time derivative of the angular position of the column structure.

The proposed method is first applied for T equal to zero to investigate the stability of the principal equilibrium solutions. In this case, the classical reduced modulus load is critical, as predicted by the dissipation based criterion for rate-dependent solids proposed by Nguyen and Radenkovic (1975). For arbitrary values of T, the stability of principal trajectories depends not only on T but also on the perturbation size. If that size is sufficiently small to prevent any unloading at the onset of perturbation, the stability threshold obtained is then called the rate-dependent tangent modulus load. It takes the value of the classical tangent modulus load for T tending to zero, is a decreasing function of T, and is independent of the value of the perturbation size. If the perturbation leads to partial unloading at the onset, the stability threshold found is called the rate-dependent reduced modulus load. It is also a decreasing function of T and a nonlinear function of the imperfection size. For the first (discrete) model, it is found that the limit for vanishing values of T of this rate-dependent reduced modulus load is the classical reduced modulus load. Note that there are two expressions for the reduced modulus loads depending on the type of boundary conditions: force or displacement control. The second (continuum) model provides further information on the singular limit of T at zero. It is found that the extent of the unloading zone at the onset for non-zero values of T is independent of the type of load control. Its value is half the column width and is identical to the one obtained for T equal to zero and displacement control. This similarity explains why the rate-dependent reduced modulus load of the second model collapses for vanishing values of T to the reduced modulus load under displacement control.

The nonlinear perturbation analyses, conducted by numerical means, always confirm the initial verdict of the linear stability criterion. The nonlinear response of the structures for longer time is of course considerably more complex. The structure can either continue to develop an instability as predicted at the onset or find a stable equilibrium which acts as attractor. Once perturbed, a linearly stable column could also develop an instability due to nonlinear effects. It turns out that, for small values

of T, the best way to understand this nonlinear behavior is to use the bifurcation equilibrium diagrams of the rate-independent column. The interpretation of the nonlinear results are similar for larger values of T, with the addition of the classical delay in the instability development. It should also be noted that those linear and nonlinear stability results are found to be in agreement with the outcome of imperfection sensitivity analyses. For example, we do find that the imperfection angle has a rate which increases at a load which is a decreasing function of T and tends to the tangent modulus load for vanishing T. This trend is similar to the dependence of our rate-dependent tangent modulus load to T. The initial imperfection development is thus well captured by our linear criterion as long as the internal variables of the model do not differ substantially from the values taken along the fundamental trajectories. This is certainly the case for large values of T for which the solution for the imperfect column remains close to the fundamental solution well past the classical tangent and reduced modulus loads.

The stability criterion proposed can be generalized to continua, as it is sketched here and summarized by Triantafyllidis et al. (1997). This generalization is possible because of the analogies between discrete models and continuum solids, thus justifying this first presentation of our stability criterion by means of a detailed analysis for two Shanley-type structures.

Acknowledgements

N.T. and Y.M.L gratefully acknowledged support by an unrestricted gift from ALCOA. The work of P.M. was completed during a post-doctoral appointment with the L.M.S. at the École Polytechnique, France. Y.M.L. thanks the Department of Aerospace Engineering at the University of Michigan for its hospitality during the summers of 1996–1998.

Appendix: Displacement control

The stability results for displacement control are sufficiently different from those discussed in the main text for force control to warrant their presentation in an Appendix. We restrict however the discussion to the first model and results, for the stability of equilibria and trajectories, are presented with no intermediate steps, since derivations are similar to the ones for force control. Before proceeding, a word on the rate-independent column under displacement control is necessary.

The smallest bifurcation load is independent of the boundary condition and is reached for a displacement U_T at the load P_T. Recall that loss of stability for $T = 0$ is marked by a zero slope along the bifurcated solution at the intersection with the fundamental path in the U–θ plane, as depicted in Fig. A1 for a zero stiffness of spring 3. At loss of stability, the critical force is $P_{R'}$ and the associated displacement is denoted similarly $U_{R'}$. The value of $P_{R'}$ exceeds the reduced modulus load P_R for force control and reads: $P_{R'} = P_E P_T / P_R$.

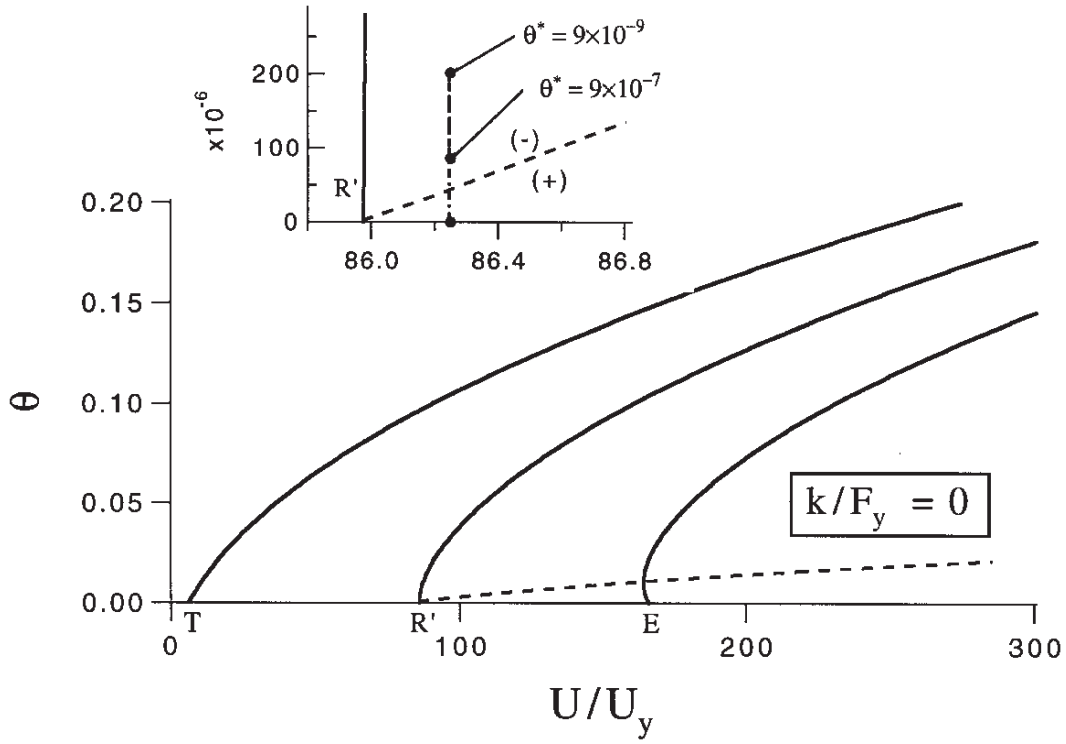

Fig. A1. Bifurcation diagram for the discrete support model under displacement control. The bifurcation paths emanating from the tangent modulus displacement and the Euler displacement are marked by T and E, respectively. The letter *R*' denotes the reduced modulus displacement for a displacement control. In the insert, the trajectories discussed in Fig. A2 are reported. The dashed curve connects the extrema of all equilibrium paths and partitions the space in stable and unstable regions, in the dissipation sense, marked by a minus and a plus sign, respectively.

A.1. *Stability of principal equilibrium solutions* (T = 0)

Stability is first discussed for the case of principal equilibria. Both linear and nonlinear results are presented. A perturbation applied at displacement level U_0 at time τ^* leaves support 1 unloading elastically while support 2 continues to accumulate permanent displacement. These two conditions are met for all time larger than τ^* investigated in this section. The linear stability criterion is again based on the second time-derivative of θ at the onset and is given by

$$\left(\frac{\mathrm{d}^2\theta}{\mathrm{d}\tau^2}\right)^* = \frac{\theta^*}{2U_{\mathrm{Y}}h}\left[1+\frac{1}{2U_{\mathrm{Y}}h}\right]\frac{P_0/P_{\mathrm{R}'}-1}{(P_0/P_{\mathrm{E}}-1)^2}. \tag{A.1}$$

The principal equilibrium branch is thus linearly stable or unstable for P_0 less or larger than $P_{\mathrm{R}'}$, respectively, in view of the change in sign at $P_{\mathrm{R}'}$ of the second derivative in (A.1).

These predictions are now validated by comparing them with the outcome of two nonlinear analyses based on the same data used to construct the bifurcation equilibrium diagram shown in Fig. A1. Two perturbations of size $9\cdot10^{-7}$ and $9\cdot10^{-9}$ are considered and are first applied at a displacement U_0 less than $U_{\mathrm{R}'}$. The results, not

presented here, confirmed the predictions of our stability criterion. The rotation rate decreases to reach a zero value signalling the approach of a new equilibrium state in the neighborhood of the perturbed equilibrium state. For a displacement U_0 larger than $U_{R'}$, the nonlinear results are more complex, as seen from Fig. A2. The normalized rotation rate $\theta_{,\tau}/|\theta^*_{,\tau}|$ is presented as a function of time and the nonlinear results (solid curves) are compared to the linear prediction (dashed line). It is seen that the rotation rate does increase initially as predicted, but there is a maximum in that rate followed by a decrease until the rotation rate reaches a zero value. This behavior is found to be independent of the imperfection size. It is similar to some observations made by Leroy (1991) and can be explained as follows with the help of the bifurcation diagram in Fig. A1. Any perturbation above $U_{R'}$ leads to an increase in the rotation of the column and the trajectories then intersect other equilibria which are stable in the dissipation sense and can act as attractors. The dashed curve in Fig. A1, partitions the set of all equilibria into a stable subset and an unstable subset marked by a minus and a plus sign in the insert. It passes through the extrema of all equilibrium paths. As the trajectories enter the stable region, the rotation rate decreases and the column selects a new equilibrium. Note the counter-intuitive result, which we shall not try to motivate, that the smallest perturbation size permits to attain an equilibrium having the largest angular position.

A.2. Stability of principal trajectories ($\mathrm{T} \neq 0$)

The displacement $U_0(\tau)$ is prescribed at a constant rate $\dot{U} \equiv V$ and has for time parameterization

$$U_0(\tau) = U_Y(T\tau + 1). \tag{A.2}$$

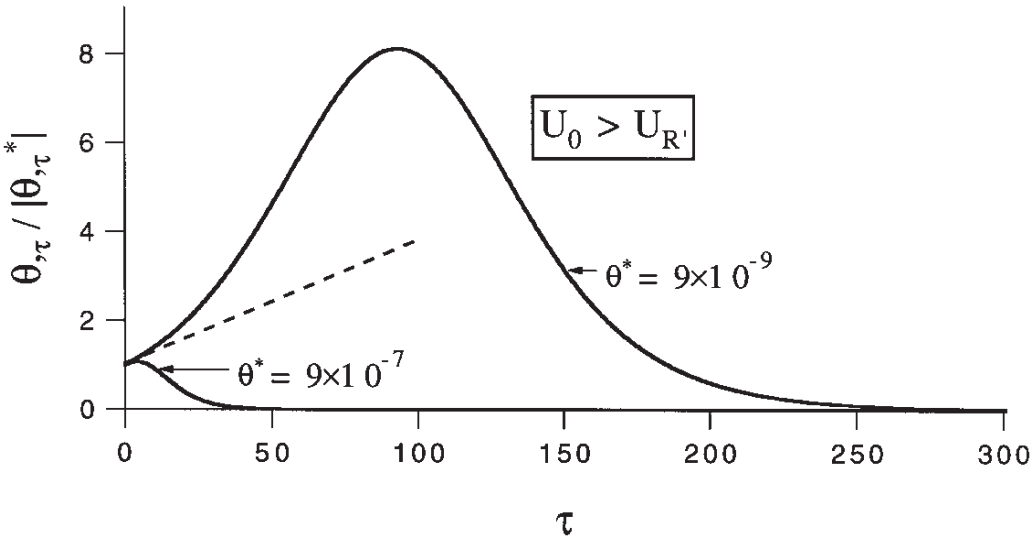

Fig. A2. The evolution with time of a perturbation from an equilibrium state for the discrete support model under displacement control. The initial rate of rotation is positive for a displacement larger than $U_{R'}$ according to the linear stability prediction which is marked by the dotted line. However, the nonlinear evolution reveals that a new equilibrium is reached since the rotation rate finally decreases to zero.

A perturbation moment $\tilde{m}$ applied to the structure results in either elastic unloading of support 1 or continuous loading of the two supports depending on the size of the perturbation. These two cases correspond to the conditions

$$\frac{U_Y T}{l(1+1/U_Y h)}\left[1-\exp\left[-(1+1/U_Y h)\tau^*\right]\right]-\theta^* \begin{cases} > 0 \Rightarrow \text{support 1 and 2 load} & \text{(Case I)} \\ < 0 \Rightarrow \text{support 1 unloads, 2 loads} & \text{(Case II)} \end{cases}. \tag{A.3}$$

They are now examined to obtain the rate-dependent tangent and reduced modulus loads for displacement control, two critical loads denoted by $P^*_{T'}$ and $P^*_{R'}$, respectively.

In Case I, both supports load at the onset and continue thereafter so that the stability limit is found to be $P^*_{T'}$ which is the force that satisfies $P_0(\tau^*) = \mathscr{P}^{*\prime}_T \equiv P^*_{T'}$ where

$$\mathscr{P}^*_{T'} \equiv P_T\left[1-\frac{3E}{P_E}\left(\frac{dP_0}{d\tau}\right)^*-\frac{F_Y hE}{EP_E^2}\left(\frac{d^2P_0}{d\tau^2}\right)^*-\left(\left(\frac{dP_0}{d\tau}\right)^*\right)^2\frac{2F_Y h}{EP_E^2}\right]\Bigg/ \left[1-\left(\frac{d^2P_0}{d\tau^2}\right)^*\frac{P_T F_Y hE}{EP_E^2}\right]. \tag{A.4}$$

This rate-dependent tangent modulus for displacement control is identical to the one obtained for force control (3.21) if the applied load is a linear function of time τ. It does converge towards the classical tangent modulus load for vanishing T and is independent of the perturbation size. It is essentially a decreasing function of T as illustrated by the dashed curve in Fig. A3. The presence of a denominator in (A.4)

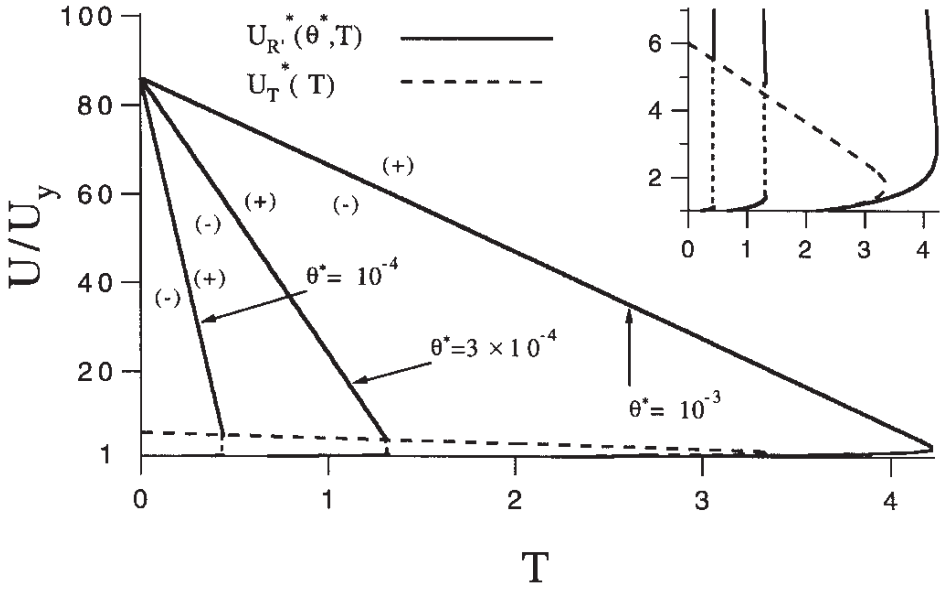

Fig. A3. The rate-dependent tangent modulus load (dashed curve) for displacement control is a function of the dimensionless number T. The rate-dependent reduced modulus load (solid curves) for the same boundary condition depends also on the perturbation size. Critical loads to be compared with those obtained for force control and presented in Fig. 5.

render the critical load a multi-valued function of T in the range of, approximately 2.2–3.2. This is the main difference between that critical load and the one found for force control as it can be seen by comparing Fig. A3 and Fig. 5.

In Case II, θ^* is large enough at τ^* to imply unloading of inelastic support 1, we are lead to the discussion of the second alternative in (A.3). The stability limit $P^*_{R'}$ is the force that satisfies $P_0(\tau^*) = \mathscr{P}^*_{R'}$ where

$$\mathscr{P}^*_{R'} = P_{R'} \times \left[\frac{1-(P_R/P_E)[q+r(1/2U_Y h-1)+(\psi/U_Y h)(3+2r)+4\psi^2/U_Y h+2\chi(1+1/U_Y h)]}{1-2\chi+(r-q)/(1+1/U_Y h)}\right],$$

$$\text{with} \quad \chi = \left(\frac{d^2 P_0}{d\tau^2}\right)^* \frac{P_T}{(P_E)^2}\frac{F_Y h}{E}, \tag{A5}$$

in which ψ, r, and q are given in (3.20), (3.25), and (3.26), respectively, with all quantities evaluated on the principal trajectory for displacement control. The critical load $P^*_{R'}$ in (A.5) is the rate-dependent reduced modulus load under displacement control. It is defined for a somewhat stronger condition than $(A.4)_2$ due to the denominator in (A.5): $1-2\chi+(r-q)/(1+1U_Y h) > 0$. The dependence of the critical load (A.5) on the imperfection size and the dimensionless number T is shown by solid curves in Fig. A3. It has the same dependence on T and perturbation size as the one observed in Fig. 5. It is a decreasing function of T tending to $P_{R'}$ in the limit of T tending to zero. Note in the insert of Fig. A3 that the rate-dependent reduced modulus load can also be multi-valued and does not exist for certain choice of imperfections size and value of T (dotted curves).

To summarize this Appendix, it should be stressed that the rate-dependent tangent modulus load for displacement control differs from the one for force control because of the different time dependence of the corresponding principal trajectory. The former provides a more general expression than the latter. The limit for vanishing T is the classical tangent modulus and load $P^*_{T'}$ decreases with T until it becomes multi-valued. The rate-dependent reduced modulus load differs form the one obtained for force control since the limit for T tending to zero is $P_{R'}$ and not P_R. It is depending on T as well as θ^* as for the force control case.

References

Asaro, R.J., 1983. Micromechanics of Crystals and Polycrystals. Adv. Appl. Mech. 23, 1–115.

Anand, L., Kim, H.K., Shawki, T.G., 1987. Onset of shear localization in viscoplastic solids. J. Mech. Phys. Solids 35, 407–429.

Bodner, S.R., Naveh, M., Merzer, A.M., 1991. Deformation and buckling of axisymmetric viscoplastic shells under thermomechanical loading. Int. J. Solids Structures 27, 1915–1924.

Carlson, R.L., 1956. Time-dependent tangent modulus applied to column creep buckling. J. Appl. Mech. 13, 390–394.

Clifton, R.J., 1978. Adiabatic shear band. Report NAMAB-356 to the US-NRC Committee on Material Response to Ultrasonic Loading Rates.
Considère, A., 1891. Résistance des pièces comprimées. Congr. Int. Proc. Constr. p. 371.
Duberg, J.E., Wilder, T.W., 1952. Inelastic column behavior. Nat. Adv. Comm. Aeron. Rep. 14.
Engesser, F., 1889. Ueber die Knickfestigkeit Geradu Stäbe. Z. Architek. Ing. 35, 455.
Hill, R., 1956. On the problem of uniqueness in the theory of a rigid/plastic solid. J. Mech. Phys. Solids 4, 247–255.
Hill, R., 1958. A general theory of uniqueness and stability in elastic/plastic solids. J. Mech. Phys. Solids 4, 247–255.
Hutchinson, J.W., 1973a. Post-bifurcation behavior in the plastic range. J. Mech. Phys. Solids 21, 163–190.
Hutchinson, J.W., 1973b. Imperfection sensitivity in the plastic range. J. Mech. Phys. Solids 21, 191–204.
Hutchinson, J.W., 1974. Plastic buckling. Adv. Appl. Mech. 14, 67–144.
Hutchinson, J.W., Neale, K.W., 1977. Influence of strain-rate sensitivity under uniaxial tension. Acta Met. 25, 839–846.
Leroy, Y.M., 1991. Linear stability analysis of rate-dependent discrete systems. Int. J. Solids Structures 27, 783–808.
Malvern, L.E., 1951. The propagation of longitudinal waves of plastic deformation in the bar of material exhibiting a strain-rate effect. J. Appl. Mech. 73, 203–208.
Mandel, J., 1971. Plasticité classique et viscoplastticité. Courses and lectures No. 97, CISM Udine, Springer-Verlag.
Massin, P.A., 1994. On the stability of strain-rate dependent solids and structures, Ph.D. Thesis, The University of Michigan.
Mikkelsen, L.P., 1993. On the analysis of viscoplastic buckling. Int. J. Solids Structures 30, 1461–1472.
Molinari, A., Clifton, R.J., 1987. Analytical characterization of shear localization in thermoviscoplastic solids. J. Appl. Mech. 54, 806–812.
Nguyen, Q.S., Radenkovic, D., 1975. Stability of equilibrium in elastic/plastic solids. I.U.T.A.M. Symposium, Marseille, pp. 403–414.
Nguyen, Q.S., 1984. Bifurcation et stabilité des systèmes Irréversibles obéissant au principe de dissipation maximale. J. Mech. Theor. Appl. 3, 41–61.
Pan, J., Rice, J.R., 1983. Rate sensitivity of plastic flow and implications for yield-surface vertices. Int. J. Solids Structures 19, 973–987.
Shanley, F.R., 1947. Inelastic column theory. J. Aeronaut. Sci. 14, 261–267.
Triantafyllidis, N., Leroy, Y.M., 1994. Stability of a frictional material layer resting on a viscous half-space. J. Mech. Phys. Solids 42, 51–110.
Triantafyllidis, N., Massin, P., Leroy, Y.M., 1997. A sufficient condition for the linear instability of strain-rate dependent solids. C.R. Acad. Sci. Par., Série II 324, 151–157.
Tvergaard, V., 1985. Rate-sensitivity in elastic–plastic panel buckling. Aspects of the Analysis of Plate Structures, W.A. Wittrick Volume, pp. 293–308.
Von Kàrmàn, T., 1910. Untensuchungen üder Knickfestigkeit, Mitteilungen üder Forschungsarbeiten. Ver. Deut. Ing. 81.
Von Kàrmàn, T., 1947. Discussion of "inelastic column theory theory". J. Aeronaut. Sci. 14, 267–268.